# Attributing the urban-rural contrast of heat stress simulated by a global

<sub>2</sub> model

Yue Qin,<sup>a</sup> Weilin Liao,<sup>b</sup> Dan Li<sup>a</sup>

- a Department of Earth and Environment, Boston University, Boston, Massachusetts, USA
- <sup>b</sup> Guangdong Key Laboratory for Urbanization and Geo-simulation, School of Geography and
- 6 Planning, Sun Yat-sen University, Guangzhou, China

7 Corresponding author: Yue Qin, yueqin@bu.edu

ABSTRACT: The Two-Resistance Mechanism (TRM) attribution method, which was designed to analyze the urban-rural contrast of temperature, is improved to study the urban-rural contrast 9 of heat stress, which better represents the human thermal comfort. The improved method can be 10 applied to diagnosing any heat stress index that is a function of temperature and humidity. As an example, in this study we use it to analyze the summertime urban-rural contrast of Simplified 12 Wet Bulb Globe Temperature (SWBGT) simulated by the Geophysical Fluid Dynamics Laboratory 13 land model coupled with an urban canopy model. We find that the urban-rural contrast of SWBGT is primarily caused by the lack of evapotranspiration in urban areas during the daytime and the release of heat storage during the nighttime, with the urban-rural differences in aerodynamic 16 features playing either positive or negative roles depending on the background climate. Compared 17 to the magnitude of the urban-rural contrast of temperature, the magnitude of the urban-rural 18 contrast of SWBGT is damped due to the moisture deficits in urban areas. We further find that the 19 urban-rural contrast of 2-m air temperature/SWBGT is fundamentally different from that of canopy 20 air temperature/SWBGT. Turbulent mixing in the surface layer leads to much smaller urban-rural contrasts of 2-m air temperature/SWBGT than their canopy air counterparts.

SIGNIFICANCE STATEMENT: Heat leads to serious public health concerns but has an uneven effect on urban and rural areas. Our study explains the magnitude and pattern of the simulated urban-rural contrast in heat stress at the global scale and improves an attribution method to quantify which biophysical processes are mostly responsible for the simulated urban-rural contrast in heat stress. We highlight two well-known causes of higher heat stress in cities: the lack of evapotranspiration and the stronger release of heat storage. Meanwhile, we draw attention to the vegetation types in rural areas, which determine the urban-rural difference in surface roughness and significantly affect the urban-rural difference in heat stress. Lastly, we find the urban-rural contrasts of 2-m air temperature/SWBGT are largely reduced relative to their canopy air counterparts due to the turbulent mixing effect.

## 1. Introduction

Prolonged exposure to heat leads to serious health problems such as heat exhaustion, heatstroke, 34 and heart diseases (Matthies et al. 2008). In 2003 and 2010, Europe and Russia experienced unprecedented heatwaves, causing around 40,000 and 55,000 deaths, respectively (Robine et al. 36 2008; Barriopedro et al. 2011). More recently in June 2021, the Pacific Northwest of the U.S. 37 and Canada experienced record-breaking high temperatures far above 104°F, leading to spikes in death and sharp increases in hospital visits (World Meterological Organization 2021). Heat is now 39 widely recognized as the number one weather killer in the U.S. (National Weather Service 2021). 4۱ Urban residents are often believed to experience higher heat stresses due to the higher temperatures in cities compared to the surrounding suburban and rural areas, which is known as the urban heat island (UHI) effect. Much effort has been made to understanding the influence of cities on weather and climate (Howard 1833; Landsberg 1981; Oke 1978; Seto and Shepherd 2009, and references therein), especially the UHI effect (Oke 1981, 1982; Yow 2007; Grimmond 2007; McCarthy et al. 2010; Oleson 2012). Nowadays it is known that the UHI effect is caused by many factors, including the lack of vegetation, the use of man-made materials with large thermal admit-47 tance, the radiative trapping effect of the three-dimensional urban canyon, and the anthropogenic heat emissions in cities (Oke et al. 2017). Increasingly sophisticated urban parameterizations have been developed to represent urban land surface and hydrological processes in numerical weather prediction models, global climate models, and earth system models, allowing the simulation of UHI intensities across time and space (Masson 2000; Kusaka et al. 2001; Oleson et al. 2008b,a; Grimmond et al. 2010, 2011; Oleson et al. 2011; Li et al. 2016a,b; Best and Grimmond 2015).

However, ambient temperature is not the only environmental component of heat stress (Fanger 1972). When considering the human thermal comfort and heat-related health issues, it is often important to also consider humidity because evaporation of sweat is a primary method for the human body to dissipate heat (Sherwood and Huber 2010). Although the urban temperature is generally higher than the rural temperature, the humidity levels in cities are often lower than those in rural areas (Oke et al. 2017), offsetting some of the enhanced heat stresses induced by the UHI effects (Chakraborty et al. 2022). Other factors such as radiation and wind speed also play important roles (Fanger 1972) and a large number of heat stress indices exist in the literature with different assumptions built into them (Anderson et al. 2013; Buzan et al. 2015).

In the climate modeling literature, a primary focus of previous studies has been quantifying how heat stress changes under a warming climate (Willett and Sherwood 2012; Dunne et al. 2013; Zhang et al. 2021). Only a handful of studies specifically examined the urban-rural contrast of heat stress and how urban and rural heat stresses respond to climate change differently. Based on simulations with the Community Climate System Model whose land component, the Community Land Model (CLM), includes an urban canopy model (UCM), Fischer et al. (2012) found that the humidity deficits offset the enhanced heat stresses in urban areas due to the UHI effects, but only weakly. Moreover, they reported that the positive urban-rural contrast of heat stress is most pronounced at night and over mid-latitudes and subtropics. Oleson et al. (2015) examined five heat stress indices (i.e., the National Weather Service Heat Index, the Apparent Temperature, the SWBGT, the Humidex, and the Discomfort Index) over North America using CLM. They highlighted that both the present-day urban-rural contrast of heat stress and the climate change impact on heat stress are highly dependent on which heat stress index is used and the urban density.

Different from previous work which largely focused on simulating the urban-rural contrast of heat stress in historical and future climates, the goal of this study is to quantify which biophysical processes (and their parameterizations) are mostly responsible for the simulated urban-rural contrast of heat stress by a global model. The premise is that only by doing so can we explain the magnitude and pattern of the simulated urban-rural contrast of heat stress by a model, as well as the differences in the simulated results by different models. To accomplish this, we develop an attribution method

- for the urban-rural contrast of heat stress indices that are functions of temperature and humidity,
- building on a recent method (Rigden and Li 2017) that has been used to attribute the urban-rural
- contrast of temperature (or the UHI intensity). As an example, we apply the improved method to
- analyzing the urban-rural contrast of Simplified Wet Bulb Globe Temperature (SWBGT) simulated
- by the Geophysical Fluid Dynamics Laboratory land model coupled with a UCM.
- Here we note that recent studies reported biases associated with the SWBGT relative to the web-
- bulb globe temperature (WBGT) (Grundstein and Cooper 2018; Kong and Huber 2022) because
- <sub>89</sub> the SWBGT does not consider wind and radiation factors which could vary locally depending
- on the vegetation density and/or land surface type (Middel et al. 2021). Nonetheless, the use of
- SWBGT in this study simply serves as an example to demonstrate how the improved method can
- be applied to analyzing any heat stress indices as long as they are only functions of temperature
- and humidity, including the National Weather Service Heat Index, the Apparent Temperature, the
- Humidex and so on (Anderson et al. 2013). The improved method does not apply to heat stress
- 95 indices that are also functions of wind speed and radiation (e.g., the WBGT and the Discomfort
- Index), the attribution analysis of which is left for future studies.
- The paper is organized as follows: Section 2 describes the model simulations and the attribution
- method; Section 3 discusses the results; Section 4 concludes the study; Section 5 discusses the
- 99 implications.

#### 2. Methods

#### a. Model Simulations

In this study, we use outputs from an offline global simulation conducted with the Geophysical Fluid Dynamics Laboratory (GFDL) land model (LM4.0), which is coupled with a UCM. The simulation, at a resolution of 2 by 2.5 degrees, is forced by a 50-year (1949-2000), 3-hourly, 1° dataset, which is based on a combination of observational and reanalysis data (Sheffield et al. 2006). We recycle the first 30-year forcing to the period of 1700-1948 to spin up the model, and the simulation covers from 1949 to 2000. In this study, we focus on the summer seasons in 1981-2000, which are defined as June, July, and August in the Northern Hemisphere and December, January, and February in the Southern Hemisphere. We only analyze grid cells with urban fractions larger than 0.1%.

A brief description of the model structure is given here. In this modeling system, there can exist 111 five different land-use/land-cover types (i.e., natural vegetation, secondary vegetation, grassland, 112 pasture, and urban), which will be called tiles hereafter, in a grid cell. Among them, the non-urban 113 tiles (i.e., natural vegetation, secondary vegetation, grassland, and pasture) are treated as rural tiles. The urban tile includes a roof component and a canyon component. The canyon component 115 further includes the pervious ground, the impervious ground, the walls, and the vegetation inside 116 the canyon. Detailed parameterizations of physical processes in urban areas, including those associated with urban vegetation, can be found in Li et al. (2016a). Validation of the UCM's 118 performance at flux sites can be found in Li et al. (2016a). Large-scale validation of simulated 119 urban and rural temperatures can be found in Liao et al. (2021). The fraction of different tiles is 120 defined through the land cover input dataset used in the Coupled Model Intercomparison Project 121 Phase 6 protocol. Hence, the fraction of the urban land, as well as the fractions of other land types, 122 evolves in the simulation period (Li et al. 2016b). 123

Both LM4.0 and UCM can be viewed as dual-source models (Bonan 2019) in the sense that the vegetation and the soil ground for the rural land (or the building and the canyon floor for the urban 125 land) have their own energy budgets and surface temperatures (e.g., Tsoil, Tveg, Tbuilding, Tground in 126 Fig. 1a). Note that Fig. 1 is a simplified schematic and is not to scale. The urban canyon for example is actually more complicated and is composed of four facets (the wall, the impervious 128 surface at the ground, the pervious ground, and the vegetation above the pervious ground). The 129 connection between these different surface temperatures is the so-called canopy air temperature  $(T_{ca})$ , where the sensible and latent heat fluxes from different facets are aggregated and passed to the 131 atmospheric model (see Fig. 1a). The canopy air temperature is different from the air temperature 132 (denoted as  $T_a$ ) at the bottom of the atmospheric model, the height of which is usually on the order 133 of 20-50 m. The canopy air temperature is also different from the so-called 2-m air temperature  $(T_2)$ , which is computed by interpolating the surface-layer temperature profile to 2 meters above 135 the displacement height  $(z_d)$ . The  $z_d$  can be regarded as the level at which the mean drag on the 136 surface appears to act (Jackson 1981), which is close to zero if there is no canopy (vegetation or urban). The value of  $z_d$  can be on the order of 10 meters for tall canopies (Garratt 1994, Table A6). 138 Like most other land surface models, the model used here assumes that within the same grid 139

cell, urban and rural tiles share the same atmospheric conditions (see Fig. 1a). Hence atmospheric

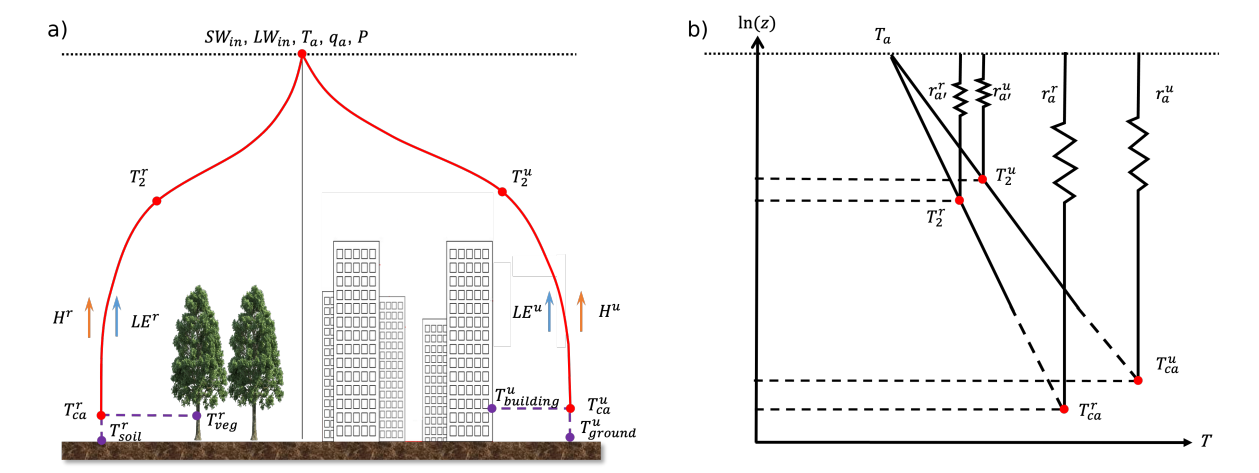


Fig. 1: (a) A schematic of the temperature and humidity definitions. The superscripts u and r represent urban and rural tiles, respectively. Subscripts ca and 2 represent canopy air and 2 meters above the displacement height, respectively.  $SW_{in}$ ,  $LW_{in}$ ,  $T_a$ ,  $q_a$ , P refer to the incoming shortwave radiation, incoming longwave radiation, the air temperature at the bottom of the atmospheric model, the specific humidity at the bottom of the atmospheric model, and the pressure, respectively. These quantities are identical for urban and rural tiles. However, urban and rural tiles have different sensible (H) and latent heat (LE) fluxes, different canopy air/2-m air temperatures as well as humidities, and different surface temperatures. (b) A schematic of how the 2-m air temperature is interpolated between the canopy air temperature and the air temperature at the bottom of the atmospheric model. Since the displacement heights and roughness lengths are different between urban and rural tiles, the canopy air and 2-m air temperature and humidity are not necessarily defined as the same physical height for urban and rural tiles.  $r_a$  refers to the bulk aerodynamic resistance to convective heat transfer between the canopy air and the bottom of the atmospheric model, while  $r'_a$  refers to the aerodynamic resistance to convective heat transfer between the 2-m level and the bottom of the atmospheric model. Although logarithmic temperature profiles are shown here for schematic purposes, the temperature profiles, in reality, are not always logarithmic due to thermal stratification.

variables  $(SW_{in}, LW_{in}, T_a, q_a, \text{ and } P)$  will not contribute to urban-rural differences when urban and rural tiles are in the same grid cell. This assumption breaks down when comparing urban and rural conditions that are in different grid cells (e.g., in high-resolution simulations) but works for 143 our analyses which focus on urban-rural differences in the same grid cell. Recall that the spatial resolution of our simulation is 2 by 2.5 degrees. When comparing urban and rural conditions that 145 are in different grid cells, this assumption can be relaxed (see an example in Wang and Li (2021)). 146 To summarize,  $T_{ca}$  and  $T_2$  are different between urban and rural tiles within the same grid cell while 147  $T_a$  is identical (Fig. 1). Similarly, we define the specific humidity at the bottom of the atmospheric model  $(q_a)$ , the 149 canopy air specific humidity  $(q_{ca})$ , and also the 2-m specific humidity  $(q_2)$ . We further define heat 150 stress indices based on these temperatures and humidities. In this study, we use the SWBGT (W) (Willett and Sherwood 2012; Fischer et al. 2012; Oleson et al. 2015), which is a unitless heat stress index calculated from ambient air temperature (T, K) and water vapor pressure (e, Pa) as

$$W = 0.567(T - 273.15) + 0.00393e + 3.94.$$
 (1)

Since the water vapor pressure is related to specific humidity(q,  $kgkg^{-1}$ ) and air pressure (P, Pa) through q = 0.622e/P, the above equation can be also written as

Therefore, due to the different temperatures/humidities defined earlier (see Fig. 1), we have three

$$W = 0.567(T - 273.15) + 0.00632Pq + 3.94.$$
 (2)

different SWBGTs: one at the bottom of the atmospheric model  $(W_a)$ , which is the same between urban and rural tiles; one in the canopy air  $(W_{ca})$ , which represents the ambient heat stress within the 158 canopy; one at 2 meters above the displacement height (W<sub>2</sub>), which lies in between the canopy and 159 the lowest level of the atmospheric model. Hereafter we refer to 2 meters above the displacement height as the 2-m level for simplicity. 161 In this study, we are interested in understanding the differences between urban and rural tiles 162 in terms of their temperatures and SWBGTs. Since the urban and rural tiles share the same 163 atmospheric conditions, the urban-rural contrasts of canopy air and 2-m air temperature and SWBGT must be caused by the urban-rural differences in surface biophysical properties such as 165 albedo, roughness length, heat capacity, etc. However, these biophysical factors make unequal 166

contributions to the urban-rural contrasts of canopy air and 2-m air temperature and SWBGT.

Quantifying the contribution of each factor requires an attribution method.

#### b. The Attribution Method

170

# 1) THE TWO-RESISTANCE MECHANISM (TRM) METHOD

The essence of the TRM method (Rigden and Li 2017) is to derive an analytical solution for the surface temperature  $(T_s, K)$  based on the energy balance equation for a bulk surface, from which the sensitivity of  $T_s$  to various biophysical factors can be directly computed. The connection between the bulk surface temperature defined in the TRM method and the canopy air and 2-m air temperature discussed above will be elaborated on later. Let us start with the energy balance equation for an infinitely thin surface layer that is horizontally homogeneous:

$$R_n = SW_{in}(1 - \alpha) + \varepsilon LW_{in} - \varepsilon \sigma T_s^4 = H + LE + G, \tag{3}$$

where  $R_n$  ( $Wm^{-2}$ ) is the net radiation,  $S_{in}$  ( $Wm^{-2}$ ) is the incoming shortwave radiation,  $L_{in}$  ( $Wm^{-2}$ ) is the incoming longwave radiation,  $\alpha$  is the surface albedo,  $\varepsilon$  is the surface emissivity,  $\sigma$  ( $Wm^{-2}K^{-4}$ ) is the Stefan-Boltzmann constant, H ( $Wm^{-2}$ ) is the sensible heat flux, LE ( $Wm^{-2}$ ) is the latent heat flux, and G ( $Wm^{-2}$ ) is the ground heat flux or heat storage. H and LE are further parameterized by the resistance concepts (Monteith and Unsworth 2008):

183

$$H = \frac{\rho c_p}{r_a} (T_s - T_a),\tag{4}$$

$$LE = \frac{\rho L_{v}}{r_{a} + r_{s}} [q^{*}(T_{s}) - q_{a}], \tag{5}$$

where  $\rho$  ( $kgm^{-3}$ ) is the air density,  $c_p$  ( $Jkg^{-1}K^{-1}$ ) is the specific heat of air at constant pressure,  $L_v$  ( $Jkg^{-1}$ ) is the latent heat of vaporization,  $q^*(T_s)$  is the saturated specific humidity at  $T_s$  following  $q^*(T_s) = 0.622e^*(T_s)/P$ , where  $e^*(T_s)$  (Pa) is the saturation vapor pressure that can be computed from  $T_s$  using the Clausius-Clapeyron relation.  $r_a(sm^{-1})$  is the aerodynamic resistance, which represents the efficiency of convective heat transfer between the surface and the atmosphere and is related to wind speed, roughness length, and stability conditions (Garratt 1994). The smaller the  $r_a$  is, the more efficient convective heat transfer becomes.  $r_s(sm^{-1})$  is the surface resistance representing how far the surface is away from saturation, which is dependent on the water availability and vegetation characteristics (Garratt 1994). The smaller the  $r_s$  is, the closer the surface is to saturation.

Substituting Eqs. 4 and 5 into Eq. 3 and linearizing the emitted longwave radiation term and the saturated specific humidity term (Rigden and Li 2017) yield

$$T_{s} - T_{a} = \frac{\lambda_{0} \{ R_{n}^{*} - G - \frac{\rho L_{v}}{r_{a} + r_{s}} [q^{*}(T_{a}) - q_{a}] \}}{1 + f_{TRM}},$$
(6)

where 
$$R_n^* = SW_{in}(1-\alpha) + \varepsilon LW_{in} - \varepsilon \sigma T_a^4$$
,  $f_{TRM} = \frac{r_0}{r_a}(1 + \frac{\delta}{\gamma} \frac{r_a}{r_a + r_s})$ ,  $\delta = \frac{de^*}{dT}|_{T_a}$ ,  $\gamma = \frac{c_p P}{0.622L_v}$ ,  $r_0 = \rho c_p \lambda_0$ ,

 $\lambda_0 = \frac{1}{4\varepsilon\sigma T_a^3}$ .

With Eq. 6, one could study the change in surface temperature  $(T_s)$  due to changes in any forcing 198 or parameter (Liao et al. 2018; Wang et al. 2019, 2020b; Moon et al. 2020). As alluded to earlier, 199 we are interested in using Eq. 6 to diagnose the differences between urban and rural tiles within the 200 same grid cell simulated by the numerical model. In this case, there are no urban-rural differences in terms of  $SW_{in}$ ,  $LW_{in}$ ,  $T_a$ ,  $q_a$ , and P. We also neglect the urban-rural difference in emissivity due 202 to its small role as demonstrated elsewhere (Liao et al. 2018; Wang et al. 2020b). Therefore, we 203 attribute the urban-rural difference in surface temperature ( $\Delta T_s$ ) to urban-rural differences in the albedo, aerodynamic resistance, surface resistance, and ground heat flux via the first-order Taylor 205 expansion, as follows: 206

$$\Delta T_s = \frac{\partial T_s}{\partial \alpha} \Delta \alpha + \frac{\partial T_s}{\partial r_a} \Delta r_a + \frac{\partial T_s}{\partial r_s} \Delta r_s + \frac{\partial T_s}{\partial G} \Delta G. \tag{7}$$

Full expressions of the partial derivatives (called the sensitivities hereafter) can be found in the Supplementary Materials. The product of the sensitivity and the difference  $(\frac{\partial T_s}{\partial X}\Delta X)$  is denoted as the contribution of the variable X to  $\Delta T_s$ .

# 210 2) Extending the TRM Method to Heat Stress

In this section, we extend the original TRM method, which was designed to study the urban-rural contrast of temperature, to study the urban-rural contrast of heat stress. For a bulk surface, the latent heat flux can also be parameterized by the difference between the surface specific humidity  $q_s$  and the atmospheric specific humidity  $q_a$  as

$$LE = \frac{\rho L_{\nu}}{r_a} (q_s - q_a). \tag{8}$$

Here  $r_s$  does not show up in the denominator because the actual specific humidity at the surface  $(q_s)$ , instead of the saturated surface specific humidity, is used. Comparing Eq. 8 to Eq. 5 gives

$$q_s = \frac{r_a}{r_a + r_s} [q^*(T_s) - q_a] + q_a.$$
 (9)

Analogous to the attribution of urban-rural difference in surface temperature, the urban-rural difference in the surface specific humidity can be expressed as

$$\Delta q_s = \frac{\partial q_s}{\partial \alpha} \Delta \alpha + \frac{\partial q_s}{\partial r_a} \Delta r_a + \frac{\partial q_s}{\partial r_s} \Delta r_s + \frac{\partial q_s}{\partial G} \Delta G. \tag{10}$$

Furthermore, based on Eq. 2, the urban-rural difference in surface SWBGT can be expressed as

$$\Delta W_s = 0.567 \Delta T_s + 0.00632 P \Delta q_s, \tag{11}$$

where  $\Delta T_s$  and  $\Delta q_s$  are from Eq. 7 and Eq. 10, respectively. Namely, the contribution of the generic variable X to  $\Delta W_s$  can be expressed as  $(0.567 \frac{\partial T_s}{\partial X} + 0.00632 P \frac{\partial q_s}{\partial X}) \Delta X$ .

As mentioned earlier, although this study only analyzes the SWBGT, the methodology can be 222 applied to other heat stress indices (e.g., the National Weather Service Heat Index, the Apparent 223 Temperature, the Humidex). Some of these indices are functions of relative humidity and/or 224 dew point temperature, but since relative humidity and dew point temperature are functions of temperature and specific humidity (with given pressure), they pose no additional challenge for this 226 method. In general, if a heat stress index (HS) can be expressed as HS = f(T,q), where f is a 227 known function, its change can thus be linked to changes in T and q through  $\Delta HS = \frac{\partial f}{\partial T}\Delta T + \frac{\partial f}{\partial q}\Delta q$ . Furthermore, the attribution method can be further improved to study mixed effects between 229 temperature and humidity by using second-order (or higher-order) Taylor expansion (see Chen 230 et al. 2020) through  $\Delta HS = \frac{\partial f}{\partial T}\Delta T + \frac{\partial f}{\partial q}\Delta q + \frac{1}{2}\left[\frac{\partial^2 f}{\partial T^2}(\Delta T)^2 + \frac{\partial^2 f}{\partial q^2}(\Delta q)^2 + 2\frac{\partial^2 f}{\partial T\partial q}\Delta T\Delta q\right]$ . In the present 231 study, we only focus on the first-order Taylor expansion while neglecting the second- and higher-232 order terms and the mixed effects, because these terms are usually of smaller magnitude relative 233 to the first-order terms. However, they can be important when the assumptions underlying Taylor 234 expansion start to break down (e.g., when the urban-rural differences of biophysical factors are no longer sufficiently small) or when one is specifically interested in the coupling and interaction of 236 the biophysical factors. 237

We need to address the following three questions before applying the attribution method discussed above to diagnosing the numerical model outputs. First, which temperature and SWBGT in the numerical model represent the bulk surface temperature ( $T_s$ ) and the bulk surface SWBGT ( $W_s$ ) in the attribution method, respectively? Second, at which time scale should the attribution analysis be conducted? Third, how to ensure that the attribution method reasonably captures the simulated

3) Application of the Attribution Method to Diagnosing the Numerical Model Outputs

urban-rural differences in  $T_s$  and  $W_s$  by the numerical model? In this section, we address these

three questions.

238

There is no single correct answer to the question of which temperature in the numerical model 246 represents (or approximates) the bulk surface temperature  $(T_s)$  in the attribution method. In our 247 opinion, the best approximation for this particular numerical model is the canopy air temperature. 248 There are two reasons supporting this argument (with more details presented in the Supplementary Materials). First, the total surface sensible heat flux is usually computed based on the difference 250 between the canopy air temperature and the air temperature at the bottom of the atmospheric model 251 in numerical models such as the LM4.0 and UCM used here. Therefore, from the atmospheric 252 model's perspective, the canopy air temperature is the temperature at which the total surface 253 sensible heat flux is generated (or at which the different heat sources on the land are aggregated). 254 In other words, the canopy air temperature would be identical to the surface temperature for a 255 bulk surface with the same total sensible heat flux and thermal roughness length (Garratt 1994). 256 Second, the canopy air temperature agrees reasonably well with the radiative surface temperature 257 in our simulation, which can be inferred from the outgoing longwave radiation with the aid of the 258 Stefan-Boltzmann law (see Fig. S1 in the Supplementary Materials). This is consistent with the findings in Li and Bou-Zeid (2014). 260

To proceed, we will use the canopy air temperature  $(T_{ca})$  to approximate  $T_s$  in the TRM attribution 261 method. Similarly, we also use the canopy air humidity  $(q_{ca})$  to represent  $q_s$  and use the extended TRM attribution method (Eq. 11) for analyzing the canopy air SWBGT. The other variables needed 263 for the attribution can then be derived. For example, the aerodynamic resistance and the surface 264 resistance are inferred using Eqs. 4 and 5, given the simulated  $T_{ca}$ , H and LE, and the forcing variables  $T_a$  and  $q_a$ . The albedo is inferred using the outgoing and incoming shortwave radiation, 266 and the ground heat flux is a default output. Note that sometimes the inferred  $r_a$  is negative when 267 applying the TRM method (or other similar methods such as the Intrinsic Biophysical Mechanism, 268 see Chen and Dirmeyer (2016)) to diagnosing numerical model outputs because numerical models are often dual- or multi-source models while these attribution methods are designed for a bulk 270 surface. The negative  $r_a$  (and also  $r_s$ ) are removed from our analysis, following previous work 271 (Liao et al. 2018; Wang et al. 2020b; Wang and Li 2021).

In terms of time scales, the default outputs are 3-hourly, consistent with the temporal resolution of the forcing. They are first separated into daytime and nighttime data. For simplicity, we assume that daytime is when the incoming shortwave radiation is greater than 25  $Wm^{-2}$  and nighttime is

when it is less than 25  $Wm^{-2}$ . We then average the 3-hourly data to monthly daytime/nighttime data and perform the attribution at the monthly scale, following Liao et al. (2020). The attribution 277 results are further averaged across 20 summers (1981 to 2000).

To ensure that the attribution method captures the simulated urban-rural differences in tempera-279 ture and SWBGT by the numerical model, the sensitivities (partial derivatives in e.g., Eq. 7) are 280 weighted averages of both urban and rural sensitivities. The weights are calibrated to best match the urban-rural differences calculated from the TRM method with those simulated by the numerical model, that is, by minimizing the root mean square error, following Liao et al. (2018). 283

#### 4) From Canopy Air Temperature/SWBGT to 2-m Air Temperature/SWBGT 284

The TRM method discussed above is used to diagnose urban-rural contrasts of canopy air 285 temperature/SWBGT. However, it is common to use the 2-m air temperature and SWBGT to quantify the near-surface microclimatic conditions in the literature, even though the interpretation of 287 '2-m' can be ambiguous over tall canopies. Here we extend the TRM method to diagnosing urban-288 rural contrasts of 2-m air temperature and SWBGT. The computation and physical interpretation of the 2-m air temperature and SWBGT are detailed in the Supplementary Materials. 290

Based on the concept of constant-flux layer, Wang and Li (2021) derived an expression for the 291 2-m air temperature  $T_2$ , as follows:

$$T_2 = \frac{r_a'}{r_a} (T_{ca} - T_a) + T_a, \tag{12}$$

where  $r'_a$  is the aerodynamic resistance to convective heat transfer between the 2-m level and the 293 atmosphere (see the right panel of Fig. 1). With this expression, the sensitivities of  $T_2$  to various biophysical factors can be computed. Similarly, one can derive the sensitivities of 2-m specific humidity using the bulk parameterization for latent heat flux, and thus the 2-m SWBGT (detailed 296 in the Supplementary Materials).

#### 3. Results 298

281

Fig. 2 and Fig. 3 show the simulated urban-rural differences of canopy air temperature ( $\Delta T_{ca}$ , 299 Fig. 2a, b), canopy air SWBGT ( $\Delta W_{ca}$ , Fig. 2c, d), 2-m air temperature ( $\Delta T_2$ , Fig. 3a, b), and 2-m 300 SWBGT ( $\Delta W_2$ , Fig. 3c, d) during the daytime and nighttime, respectively. It is evident that the

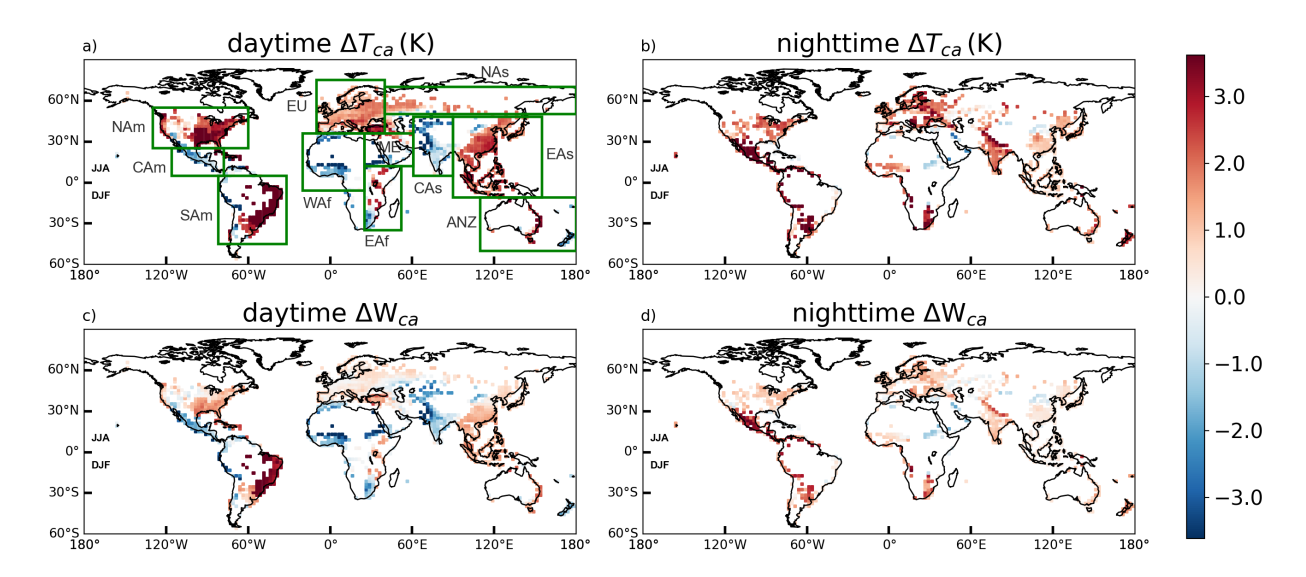


Fig. 2: Simulated urban-rural contrasts ( $\Delta$  = urban - rural) of (a) daytime canopy air temperature ( $T_{ca}$ ), (b) nighttime canopy air temperature, (c) daytime canopy air SWBGT ( $W_{ca}$ ), and (d) nighttime canopy air SWBGT. The green boxes in (a) define the boundary of 11 regions: North America (NAm), Central America (CAm), South America (SAm), Europe (EU), Western Africa (WAf), Eastern Africa (WAf), Middle East (ME), North Asia (NAs), Central Asia (CAs), Eastern Asia (EAs), Australia/New Zealand (ANZ).

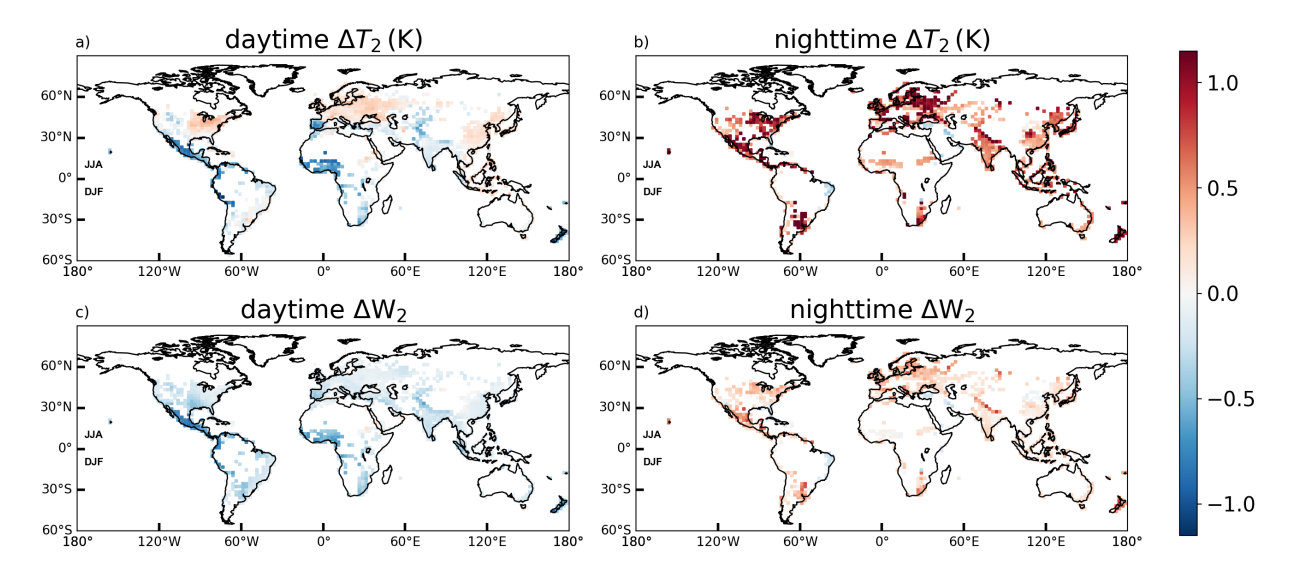


Fig. 3: Simulated urban-rural contrasts ( $\Delta$  = urban - rural) of (a) daytime 2-m air temperature ( $T_2$ ), (b) nighttime 2-m air temperature, (c) daytime 2-m SWBGT ( $W_2$ ) and (d) nighttime 2-m SWBGT.

simulated urban-rural contrasts show large differences between daytime and nighttime, as well as strong spatial variabilities. We will first focus on understanding the general patterns in the daytime and nighttime results (Sections 3.a-3.c), and then discuss the spatial variability (Section 3.d).

For  $\Delta T_{ca}$  and  $\Delta W_{ca}$ , the most striking feature is that some regions exhibit negative values in 305 the daytime, such as Central America, West Africa, and Central Asia. As proposed elsewhere 306 (Carnahan and Larson 1990), the urban heat sink could occur during the daytime when urban surfaces have greater heat absorption and rural areas have dry, bare soil with low thermal inertia and low evaporative cooling. At night,  $\Delta T_{ca}$  and  $\Delta W_{ca}$  are mostly positive. By comparing the 309 results for  $\Delta T_{ca}$  and  $\Delta W_{ca}$ , one can see that  $\Delta W_{ca}$  is smaller than  $\Delta T_{ca}$ , especially in areas with 310 positive values of both. This is due to the humidity deficits in urban areas, namely, urban areas are 311 generally hotter but drier, as alluded to earlier. Hence the enhanced heat stresses in the urban areas 312 by the positive UHI effects are partially offset by the humidity deficits. 313

Comparing Fig. 3 (a, b) to Fig. 2 (a, b) reveals that  $\Delta T_2$  has similar spatial patterns as  $\Delta T_{ca}$  but with 314 much smaller magnitude and with more negative values during the daytime. The smaller magnitude 315 of  $\Delta T_2$  than  $\Delta T_{ca}$  is due to the role of turbulent mixing. In the surface layer (between the land 316 model and the lowest level of the atmospheric model), turbulent eddies transport mass, momentum, 317 and heat from the surface to the atmosphere or vice versa (Stull 1988). The turbulent transport is responsible for the logarithmic profiles under neutral conditions (or the profiles described by 319 Monin-Obukhov similarity theory under thermally stratified conditions) in the surface layer, as 320 illustrated in Fig. 1b. Although urban land has biophysical properties that are different from those of rural land and thus the surface conditions differ between the urban and rural land, such 322 differences become smaller as the urban and rural fluxes become mixed and eventually disappear 323 when the fluxes reach the lowest level of the atmospheric model. 324

With the turbulent mixing effects and the humidity deficits in urban areas, the daytime  $\Delta W_2$  (Fig. 3c) turns into negative worldwide. Although the nighttime  $\Delta W_2$  (Fig. 3d) remains positive, the mixing effects cause its magnitude to be smaller than  $\Delta W_{ca}$ .

We should highlight that  $\Delta T_2$  and  $\Delta W_2$  are not necessarily fair indicators of near-surface air temperature and heat stress differences between urban and rural areas, because  $T_2$  and  $W_2$  are defined at 2 meters above the displacement height and the urban displacement height is often much larger than the rural counterpart except for forests (Oke et al. 2017). As a result, the height at which the 2-m air temperature is defined is usually different between urban and rural areas. We did not correct the definition of the '2-m' level to be consistent with the literature, but we note that some models try to correct such effects by computing new temperature/humidity variables at 2 meters

329

330

332

333

above the ground (Meili et al. 2020) and other models such as CLM have the 2-m air temperature defined differently for urban and rural areas. In CLM (Oleson et al. 2013),  $T_{ca}$  is assigned to the 2-m air temperature directly for urban areas while for rural areas the 2-m air temperature is defined at 2 meters above the displacement height and interpolated between  $T_{ca}$  and  $T_a$ . This partly explains why our results of  $\Delta T_2$  are different from those from CLM (Oleson et al. 2011).

Perhaps what is more meaningful is the comparison between the daytime and nighttime results. For  $T_{ca}$  and  $W_{ca}$ , the urban-rural contrasts are stronger during the daytime; while for  $T_2$  and  $W_2$ , the urban-rural contrasts are stronger during the nighttime. This is consistent with previous work showing that the surface UHI is often stronger during the daytime, while the near-surface UHI tends to be stronger at night (Oke et al. 2017; Stewart et al. 2021; Venter et al. 2021).

It is important to stress that the aim of this study is not to validate the results shown in Fig. 2 and Fig. 3. Instead, the goal is to quantify the contributions of different biophysical factors to the simulated  $\Delta T_{ca}$ ,  $\Delta W_{ca}$ ,  $\Delta T_2$ , and  $\Delta W_2$  using the improved TRM attribution method. In the following, we first present the sensitivities of  $T_{ca}$ ,  $W_{ca}$ ,  $T_2$ , and  $W_2$  to biophysical factors, followed by the urban-rural differences in biophysical factors. The products of the sensitivities and the urban-rural differences, which represent the contributions of different biophysical factors, are then presented. Lastly, the regionally averaged attributions are shown to highlight the spatial variability.

### 352 a. Sensitivities to Biophysical Factors

362

# 353 1) Sensitivities of Heat Stress at the Canopy Air Level

As the first step, we calculate the sensitivities of canopy air temperature ( $T_{ca}$ ) and canopy air SWBGT ( $W_{ca}$ ) to biophysical factors (namely, albedo, aerodynamic resistance, surface resistance, and heat storage) based on the formulae presented in the Supplementary Materials. Because the results of  $T_{ca}$  and  $W_{ca}$  are similar in terms of the global patterns, we only present the results for  $W_{ca}$  here (Fig. 4) while the sensitivities of  $T_{ca}$  to biophysical factors can be found in the Supplementary Materials (see Fig. S2).

First, the sensitivity of  $W_{ca}$  to albedo is negative worldwide during the daytime and is close to zero at night, as shown in Fig. 4(a, b). Intuitively, the larger the surface albedo, the more solar radiation

is reflected and the lower the  $T_{ca}$ , as well as the  $W_{ca}$ , which explains the negative sensitivity in the

daytime. Fig. 4(c, d) present the sensitivity of canopy air heat stress to aerodynamic resistance

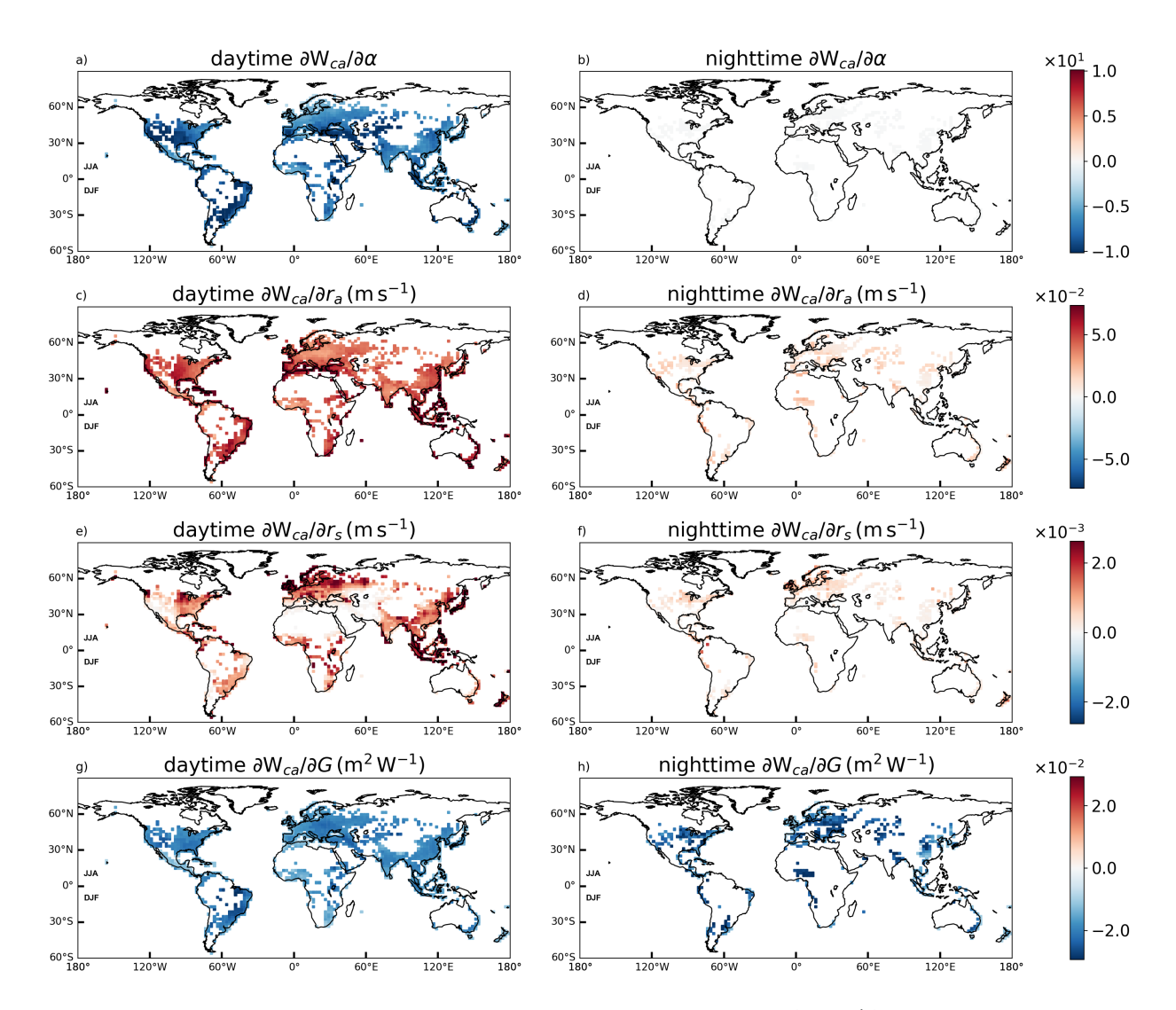


Fig. 4: The sensitivities of canopy air SWBGT to (a, b) albedo  $(\partial W_{ca}/\partial \alpha)$ , (c, d) aerodynamic resistance  $(\partial W_{ca}/\partial r_a)$ , (e, f) surface resistance  $(\partial W_{ca}/\partial r_s)$ , and (g, h) heat storage  $(\partial W_{ca}/\partial G)$  during daytime (left column) and nighttime (right column).

 $(\partial W_{ca}/\partial r_a)$ . It is clear that  $\partial W_{ca}/\partial r_a$  is positive worldwide in the day while is much smaller at night. As discussed in Liao et al. (2020), the positive sensitivity during the daytime implies that when the land surface becomes less efficient in transferring sensible heat to the lower atmosphere (i.e., when  $r_a$  increases),  $W_{ca}$  tends to increase. Fig. 4e shows a positive signal of  $\partial W_{ca}/\partial r_s$  globally during the daytime, indicating that  $W_{ca}$  increases as the land surface becomes less efficient in using energy for evapotranspiration (i.e., when  $r_s$  increases). This effect is understandably small during the nighttime (see Fig. 4f) as photosynthesis stops. Lastly, Fig. 4(g, h) show the sensitivity of  $W_{ca}$  to heat storage  $(\partial W_{ca}/\partial G)$  during the daytime and nighttime, respectively. Note that the

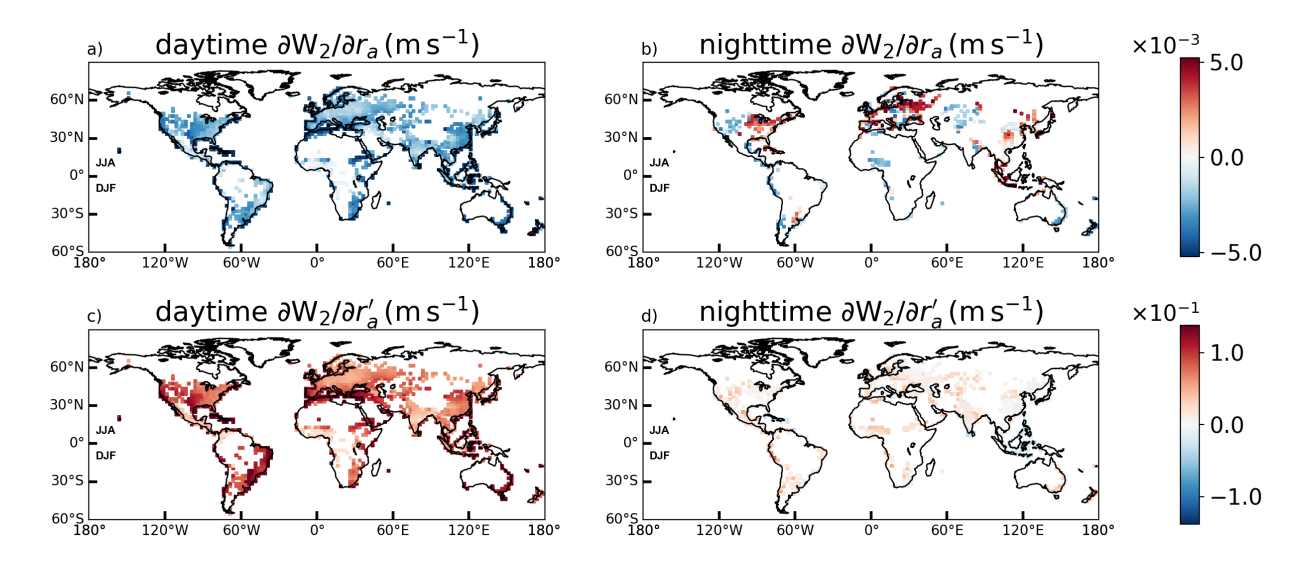


Fig. 5: The sensitivities of 2-m SWBGT to (a, b) aerodynamic resistance ( $\partial W_2/\partial r_a$ ), and (c, d) 2-m aerodynamic resistance ( $\partial W_2/\partial r_a'$ ) during daytime (left column) and nighttime (right column).

ground heat flux is defined to be positive downward and negative upward. Therefore, the fact that more ground heat flux goes downward to deeper soil layers (or built materials) during the daytime means a decrease in canopy air temperature and heat stress, leading to negative daytime  $\partial W_{ca}/\partial G$ . Conversely, the fact that more ground heat flux goes upward to the surface during the night means an increase in canopy air temperature and heat stress, also leading to negative nighttime  $\partial W_{ca}/\partial G$ . Although  $\partial W_{ca}/\partial G$  is negative for both daytime and nighttime, the magnitude of  $\partial W_{ca}/\partial G$  at night is larger than that in the day, showing a stronger effect of heat release on canopy air temperature and heat stress at night than that of heat storage during the day.

### 2) Sensitivities of Heat Stress at the 2-m Level

Similarly, we examine the sensitivity of  $W_2$  to albedo, surface resistance, and heat storage (see Fig. S3 in the supplementary materials). Compared to the results for  $W_{ca}$ , the sensitivities of  $W_2$  to albedo, surface resistance, and heat storage show very similar patterns but have a smaller magnitude, because these sensitivities are simply their counterparts for  $W_{ca}$  multiplied by the factor  $r'_a/r_a$ , which is smaller than unity (see Eqs. S17 to S20 in the Supplementary Materials).

The more complicated sensitivities are those to  $r_a$  (i.e., aerodynamic resistance between the surface and the atmosphere) and  $r'_a$  (i.e., aerodynamic resistance between the 2-m level and the atmosphere). Fig. 5a shows that during the daytime the sensitivity of  $W_2$  to aerodynamic resistance

 $(\partial W_2/\partial r_a)$  is negative. This is contrary to the positive  $\partial W_{ca}/\partial r_a$  (see Fig. 5c). That is because 389 when it is less efficient in transferring heat from the surface (or more precisely the height at which 390 the canopy air temperature is defined) to the atmosphere (i.e.,  $r_a$  increases), the air temperature 391 and heat stress in the canopy increase while the air temperature and heat stress at the 2-m level decrease. However, if it is less efficient in transferring heat from the 2-m level to the atmosphere 393 (i.e.,  $r'_a$  increases), the 2-m air temperature and heat stress increase, which explains the positive 394  $\partial W_2/\partial r'_a$  during the daytime (Fig. 5c). It should be also pointed out that  $\partial W_2/\partial r'_a$  is of larger magnitude than  $\partial W_2/\partial r_a$ , indicating that  $W_2$  is more affected by changes in  $r'_a$  than in  $r_a$ . During 396 the nighttime,  $\partial W_2/\partial r_a$  is very heterogeneous at the global scale and  $\partial W_2/\partial r'_a$  is weakly positive 397 (Fig. 5b, d).

# b. Urban-Rural Differences in Biophysical Factors

We further compare the urban-rural differences in five biophysical factors. Fig. 6(a, b) show 400 a negative contrast in albedo over most regions except for the western edge of South America, 401 Equatorial Africa, the Mediterranean region, and West Asia. The negative albedo differences imply 402 that the urban land is parameterized with a smaller albedo than the rural land in the numerical 403 model, while the positive albedo differences indicate the opposite. Although the radiative trapping effect tends to reduce the albedo of urban land, urban land does not always have a smaller albedo 405 than rural land, and the urban-rural albedo differences depend on the characteristics of urban and 406 rural land (e.g., urban form, rural vegetation type) (Oke et al. 2017). Our results here also reflect this. 408

The daytime contrast of aerodynamic resistance ( $r_a$ ) shows strong spatial variability, which is highly related to the rural vegetation type. For example, in arid regions (i.e., Central America, Middle East, and Central Asia), rural land is characterized by vegetation of low height such as shrubs, sage brushes, and grasses, which makes it less efficient for rural land to transfer sensible heat to the atmosphere than urban land. Therefore, the urban-rural contrast in aerodynamic resistance ( $\Delta r_a$ ) in drier regions tends to be negative, as opposed to more humid regions where rural land has taller vegetation and thus might have smaller  $r_a$  than adjacent urban land (i.e., positive in Fig. 6c). At night,  $\Delta r_a$  shows a negative signal almost everywhere, particularly in densely populated regions (e.g., Eastern North America, Eastern South America, Europe, East, and Southeast Asia), indicating

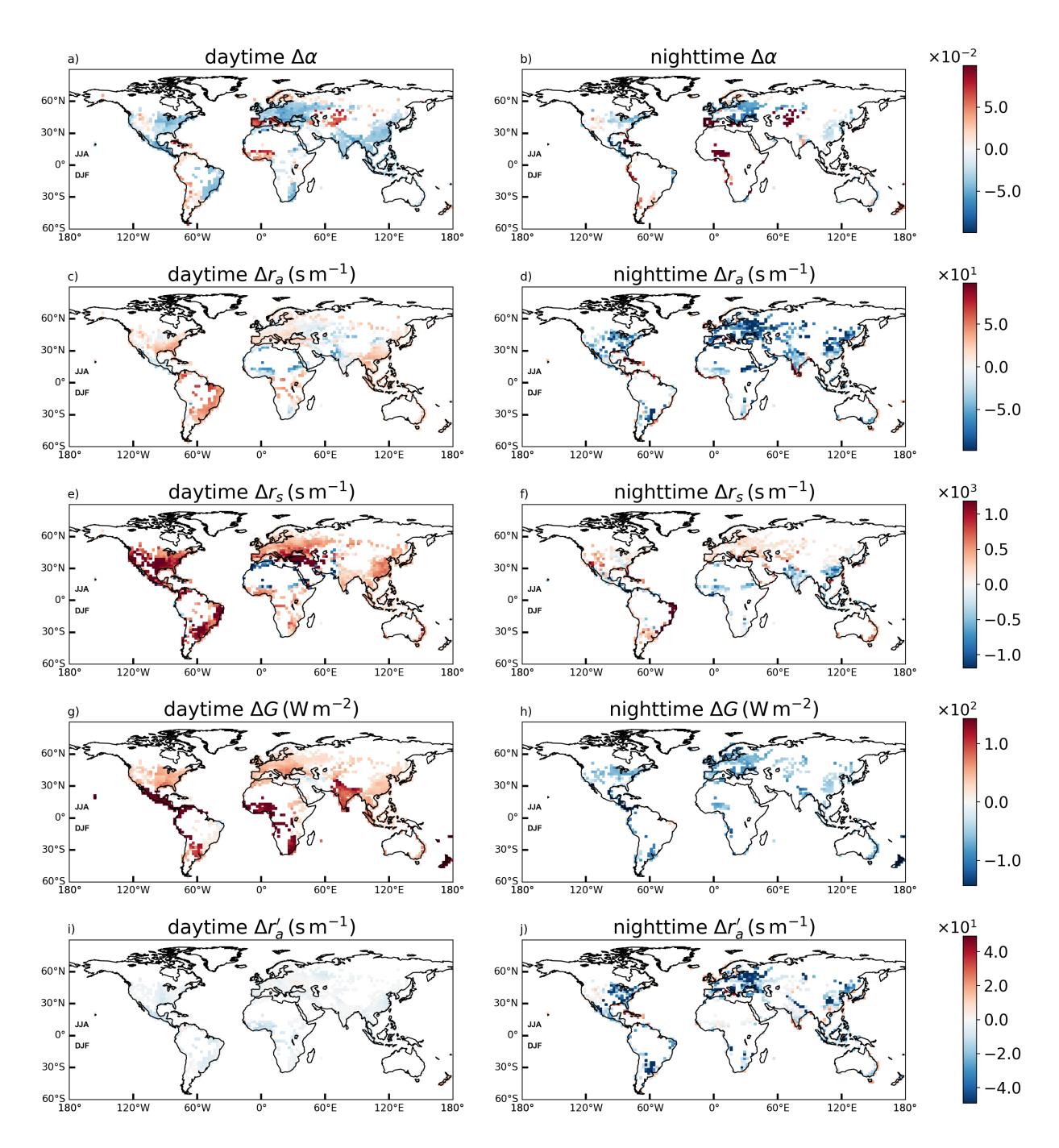


Fig. 6: The contrasts between urban and rural areas ( $\Delta$  = urban - rural) in (a, b) albedo ( $\alpha$ ), (c, d) aerodynamic resistance ( $r_a$ ), (e, f) surface resistance ( $r_s$ ), (g, h) heat storage (G) and (i, j) 2-m aerodynamic resistance ( $r'_a$ ) during daytime (left column) and nighttime (right column). Note that the  $r'_a$  is only relevant for the attribution of 2-m air temperature and 2-m SWBGT in Fig. 3.

- that cities are more efficient in transferring heat from the surface to the lower atmosphere at night.
- This is consistent with the stronger release of ground heat storage in urban areas, creating more

unstable stratification in the urban surface layer. In contrast, convective heat transfer is less efficient with the existence of a stable surface layer in rural areas. Previous field studies have confirmed a near-neutral or slightly unstable boundary layer in cities while a stable boundary layer in rural areas during nighttime (Uno et al. 1992; Dupont et al. 1999).

The daytime contrast in surface resistance  $(r_s)$  is found to be positive almost everywhere (Fig. 6e), indicating that it is much harder for urban areas to produce evapotranspiration than rural areas. The nighttime  $\Delta r_s$  is much smaller than the daytime counterpart and can be quite uncertain due to the small latent heat flux at night (Fig. 6f). The urban-rural contrast in heat storage ( $\Delta G$ ) is positive during the daytime and negative during the nighttime (Fig. 6g, h). This is caused by the larger thermal admittance of surface materials in cities, which allows urban surfaces to store more heat during the day and thus release more heat at night (Oke et al. 2017; Grimmond and Oke 1999).

The extra factor that only appears in the attribution of urban-rural contrasts of 2-m air temperature 431 and SWBGT is the 2-m layer aerodynamic resistance  $(r'_a)$ . We find that  $\Delta r'_a$ , being negative, is 432 weaker than  $\Delta r_a$  during the daytime (see Figs. 6i and 6c), implying that most of the resistance to convective heat transfer during the daytime lies between the surface and the 2-m level. This 434 is because the size of turbulent eddies responsible for heat transfer scales with the distance from 435 the surface (Katul et al. 2011; Li 2021). Between the surface and the 2-m level, the eddies are smaller and thus heat transfer is less efficient than their counterparts between the 2-m level and the 437 atmosphere. During the night, the magnitude of  $\Delta r'_a$  increases and  $\Delta r'_a$  is similar to  $\Delta r_a$  (see Figs. 6j 438 and 6d), suggesting that most of the resistance to convective heat transfer during the nighttime lies between the 2-m level and the atmosphere. In other words, the 2-m level becomes decoupled from 440 the atmosphere due to the stable stratification, leading to stronger  $\Delta r_a'$ . 441

# 442 c. Contributions of Biophysical Factors

By multiplying the sensitivities (Fig. 4) and the urban-rural differences (Fig. 6), the contributions from these biophysical factors to the urban-rural contrast of canopy air SWBGT ( $\Delta W_{ca}$ ) are computed, as shown in Fig. 7. In the same way, we quantify the contributions to the urbanrural contrasts of 2-m SWBGT ( $W_2$ ) (see Fig. 8), canopy air temperature ( $T_{ca}$ ) (see Fig. S5 in the Supplementary Materials), and 2-m air temperature ( $T_2$ ) (see Fig. S4 and Fig. S6 in the Supplementary Materials).

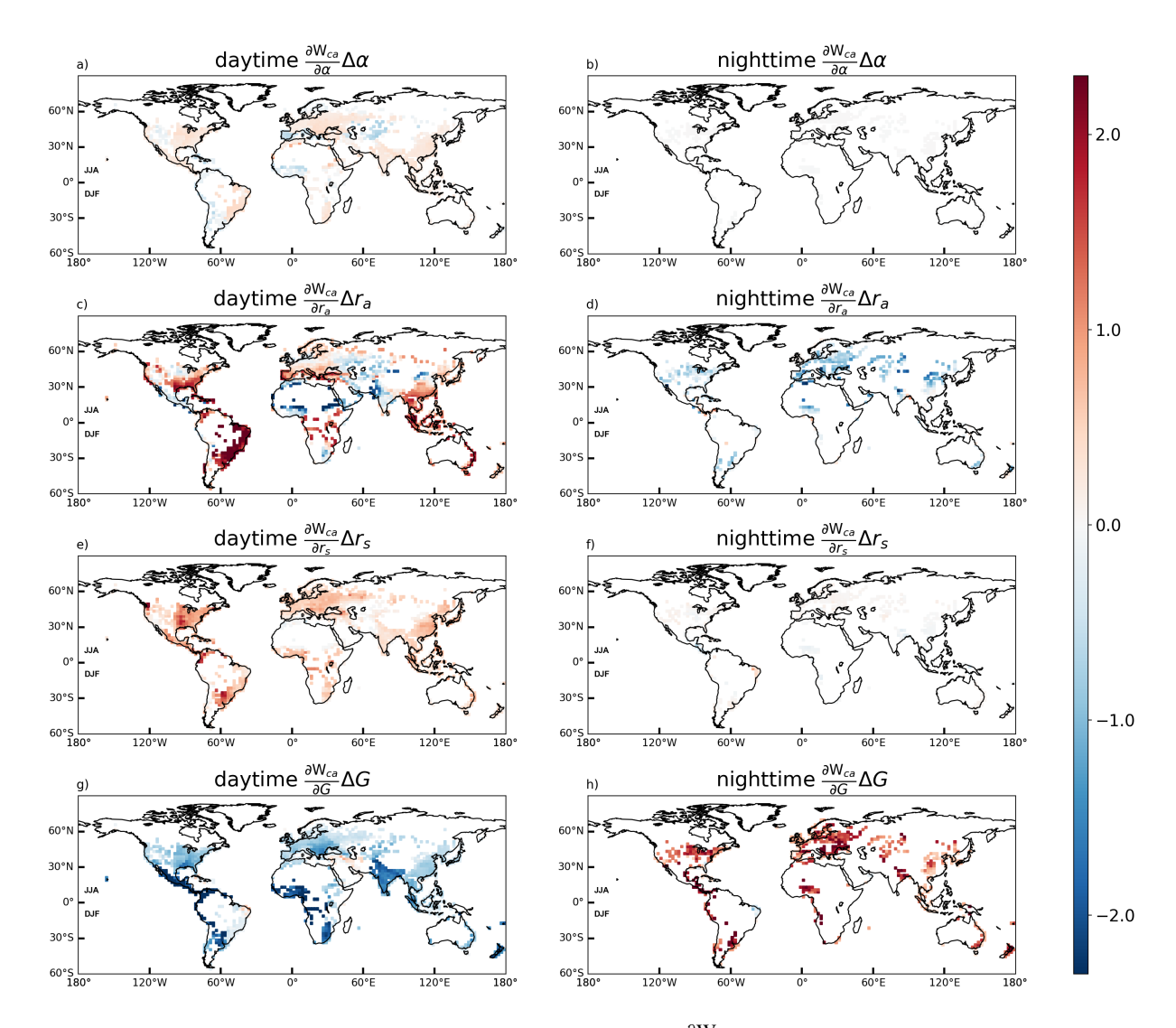


Fig. 7: The contributions to  $\Delta W_{ca}$  from (a, b) albedo  $(\frac{\partial W_{ca}}{\partial \alpha}\Delta\alpha)$ , (c, d) aerodynamic resistance  $(\frac{\partial W_{ca}}{\partial r_a}\Delta r_a)$ , (e, f) surface resistance  $(\frac{\partial W_{ca}}{\partial r_s}\Delta r_s)$  and (g, h) heat storage  $(\frac{\partial W_{ca}}{\partial G}\Delta G)$  during daytime (left column) and nighttime (right column).

Before discussing the attribution results, we first use the numerical model simulated  $\Delta W_{ca}$  (or  $\Delta T_{ca}$ ) to evaluate the TRM method by comparing the numerical model simulated results to the sum of the contributions from all biophysical components in the TRM method. It can be seen that the TRM attribution method is able to capture the numerical model simulation results with small root mean square errors (see Fig. S7 and Fig. S8 in the Supplementary Materials). Nevertheless, at the 2-m level, the TRM-modeled  $\Delta W_2$  and  $\Delta T_2$  become more scattered compared to the simulated ones, which suggests that the extension of the TRM attribution method to the 2-m level introduces

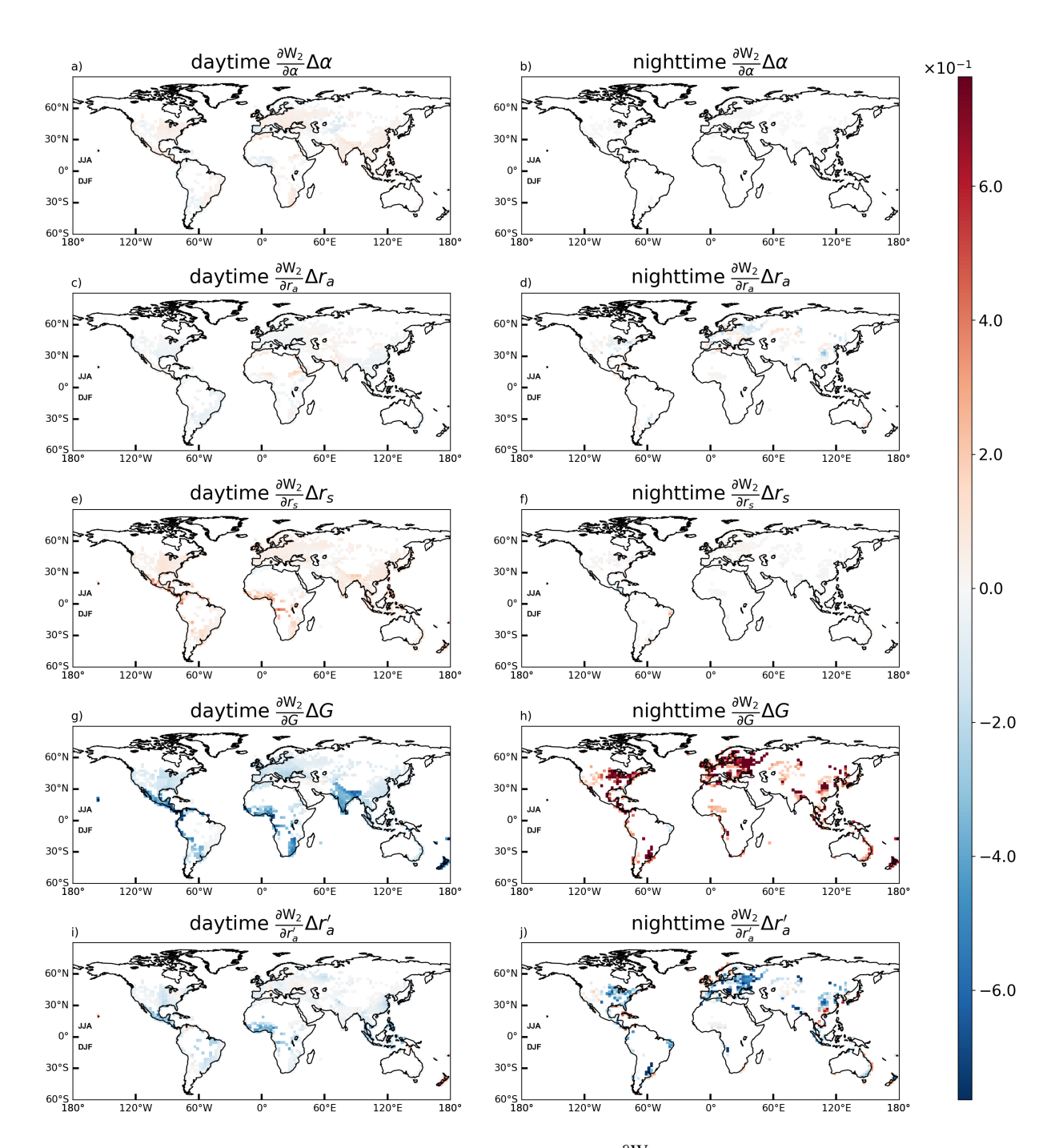


Fig. 8: The contributions to  $\Delta W_2$  from (a, b) albedo  $(\frac{\partial W_2}{\partial \alpha}\Delta\alpha)$ , (c, d) aerodynamic resistance  $(\frac{\partial W_2}{\partial r_a}\Delta r_a)$ , (e, f) surface resistance  $(\frac{\partial W_2}{\partial r_s}\Delta r_s)$ , (g, h) heat storage  $(\frac{\partial W_2}{\partial G}\Delta G)$ , and (i, j) 2-m aerodynamic resistance  $(\frac{\partial W_2}{\partial r_a'}\Delta r_a')$  during daytime (left column) and nighttime (right column).

more uncertainties. This is not too surprising considering that the magnitudes of  $\Delta W_2$  and  $\Delta T_2$  are

smaller than their canopy air counterparts.

Now let's turn to the general patterns of the attribution results (Fig. 7). Here we use the same 458 color bar for all the factors in order to highlight their relative magnitude. During the daytime, 459 albedo plays the least role in  $\Delta W_{ca}$  among all biophysical factors (see Fig. 7a, b). That is because 460 the model prescribes a very small urban-rural difference in albedo, which is on the order of  $10^{-2}$ (see Fig. 6a,b). Other factors show stronger effects. Specifically, surface resistance contributes 462 positively while heat storage contributes negatively during the daytime (see Fig. 7e, g), due to the 463 combining effect of the large sensitivities (Fig. 4) and the large urban-rural differences in terms of these two factors (Fig. 6). Daytime effects of aerodynamic resistance are more complex with strong 465 spatial variability (Fig. 7c). At night, aerodynamic resistance and ground heat storage dominate 466 the urban-rural difference in the canopy air SWBGT, with negative and positive contributions, 467 respectively (Fig. 7d,h). Albedo and surface resistance has negligible effects at night (see Fig. 7b, 468 f). The effect of ground storage shows a similar magnitude between day and night while others are 469 weaker at night than during the day. 470

Furthermore, by comparing the results of  $\Delta W_{ca}$  (Fig. 7) and  $\Delta T_{ca}$  (Fig. S5), it is evident that the general patterns are similar but the effects of all four biophysical factors on  $\Delta W_{ca}$  are reduced in terms of the magnitude due to the humidity deficits in cities. In particular, surface resistance is the most dampened component such that the magnitude of the contribution of surface resistance to  $\Delta W_{ca}$  is around 25% of that to  $\Delta T_{ca}$ . Closer inspection reveals that the magnitude of the sensitivity of  $W_{ca}$  to  $W_{ca}$  is about 25% of the sensitivity of  $W_{ca}$  to  $W_{ca}$  is about 25% of the sensitivity of  $W_{ca}$  to  $W_{ca}$  is about 25% of the sensitivity of  $W_{ca}$  to  $W_{ca}$  to  $W_{ca}$  is about 25% of the sensitivity of  $W_{ca}$  to  $W_{ca}$  is about 25% of the sensitivity of  $W_{ca}$  to  $W_{ca}$  is about 25% of the sensitivity of  $W_{ca}$  to  $W_{ca}$  is about 25% of the sensitivity of  $W_{ca}$  to  $W_{ca}$  to  $W_{ca}$  is about 25% of the sensitivity of  $W_{ca}$  to  $W_{ca}$  to  $W_{ca}$  is about 25% of the sensitivity of  $W_{ca}$  to  $W_{ca}$  to  $W_{ca}$  to  $W_{ca}$  is about 25% of the sensitivity of  $W_{ca}$  to  $W_{ca}$  to the increase in  $W_{ca}$  the increase in  $W_{ca}$  when compared to the increase in  $W_{ca}$ 

At the 2-m level, results for albedo, surface resistance, and ground storage (see Fig. 8) exhibit much smaller magnitude than those at the canopy air level due to turbulent mixing. During the daytime, the main contributors are surface resistance (positive) and ground storage (negative) and there are no significant contributions of albedo and aerodynamic resistance. Nevertheless, it is worth noting that aerodynamic resistance makes the opposite contributions to  $\Delta W_2$  and  $\Delta W_{ca}$  (c.f., Fig. 8 and Fig. 7). This is because the sensitivity of  $W_2$  to  $r_a$  has an opposite sign as the sensitivity of  $W_{ca}$  to  $r_a$  as discussed in Section 3.a. As for the 2-m aerodynamic resistance ( $r'_a$ ) (see Fig. 8i, j), it consistently exerts negative effects due to that the majority of regions displays negative urban-rural difference in  $r'_a$  (as in Fig. 6i, j). As a result, the negative contribution from ground storage

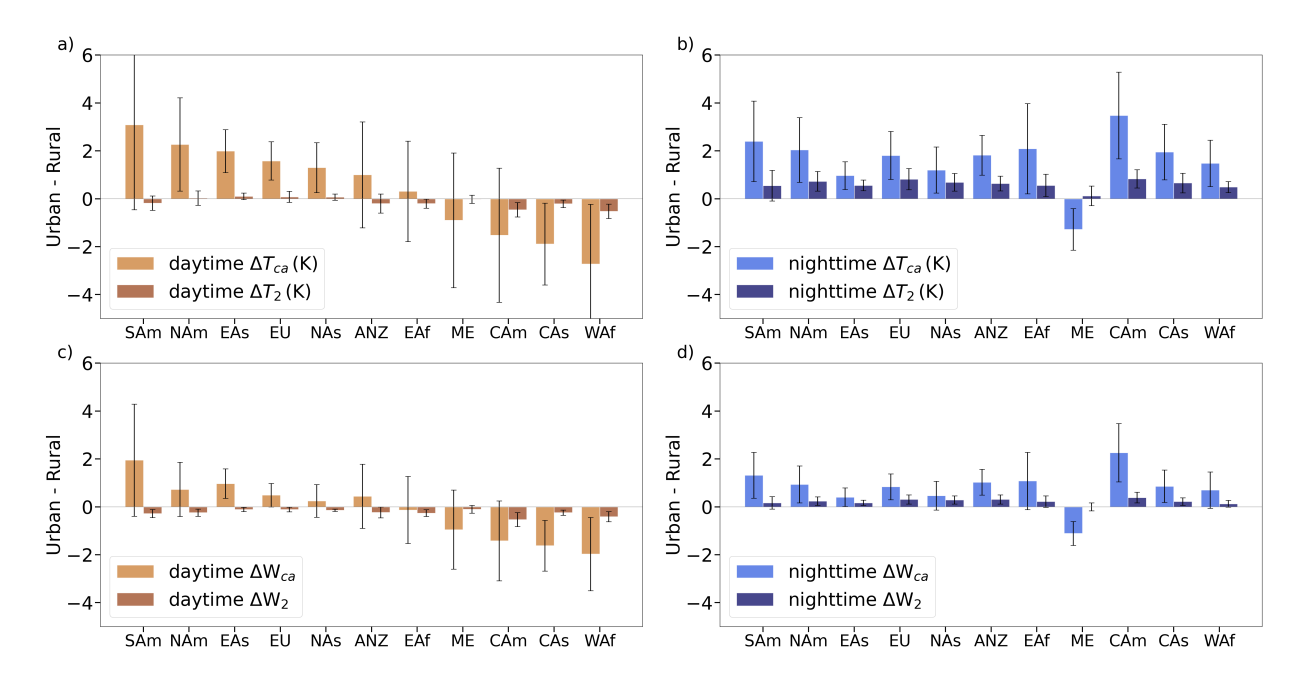


Fig. 9: Regional averages of urban-rural contrasts of (a, b) canopy air temperature ( $\Delta T_{ca}$ ) and 2-m air temperature ( $\Delta T_2$ ), (c, d) canopy air SWBGT ( $\Delta W_{ca}$ ) and 2-m SWBGT ( $\Delta W_2$ ) during daytime (left column) and nighttime (right column). The error bars are the standard error and indicate the spatial variability.

(Fig. 8g) together with the negative contribution from the 2-m aerodynamic resistance causes a negative daytime  $\Delta W_2$  (see Fig. 3c). During the night, only ground storage (positive) and the 2-m aerodynamic resistance (negative) play a role in  $\Delta W_2$  (see Fig. 8h, j).

# <sup>491</sup> d. Regionally-averaged Attributions of $\Delta T_{ca}$ , $\Delta T_2$ , $\Delta W_{ca}$ , and $\Delta W_2$

Because the urban-rural differences in temperature and SWBGT display an evident dependence 492 on geographic locations (see Figs. 2, 3), in this section results are analyzed in the manner of 493 regional averages. Region boundaries are defined in a similar way as McCarthy et al. (2010) (see Fig. 2a with the region abbreviations defined in the caption). Fig. 9 shows the regional averages 495 of  $\Delta T_{ca}$ ,  $\Delta T_2$ ,  $\Delta W_{ca}$ , and  $\Delta W_2$  during the daytime and nighttime. Comparing the upper panels 496 against the lower ones, the similarity between the averaged urban-rural contrasts of temperature 497 and SWBGT shows up clearly over all regions. The regional averages of daytime  $\Delta T_{ca}$  and  $\Delta W_{ca}$ are positive except in the Middle East, Central America, Central Asia, and West Africa, due to the 499 reasons discussed at the beginning of this section. During the nighttime, all regions but the Middle 500 East show positive values of  $\Delta T_{ca}$  and  $\Delta W_{ca}$ . In terms of the 2-m air temperature and SWBGT, the

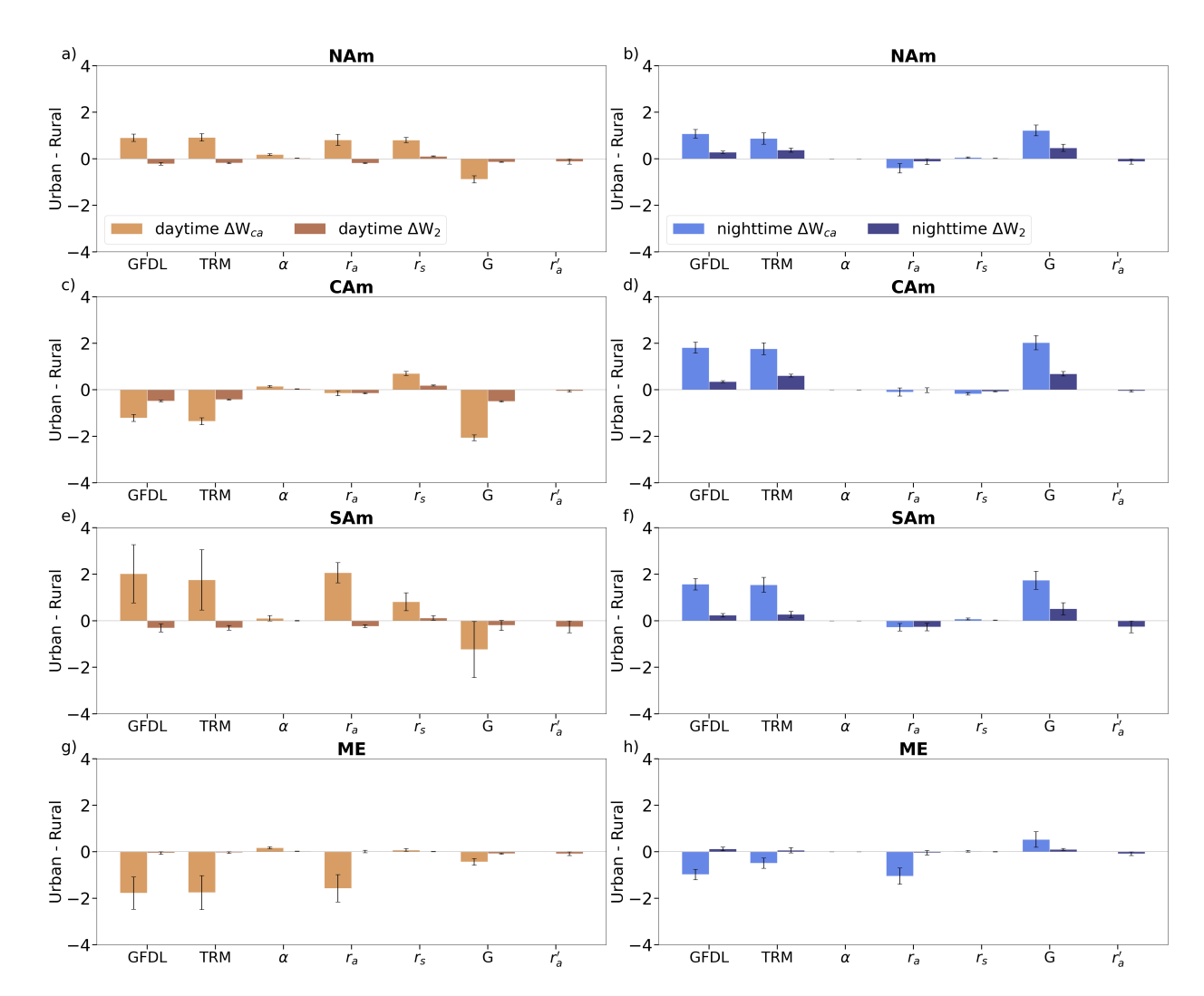


Fig. 10: Regionally-averaged attribution results for urban-rural contrasts of canopy air SWBGT ( $\Delta W_{ca}$ ) and 2-m SWBGT ( $\Delta W_2$ ) over (a, b) North America (NAm), (c,d) Central America (CAm), (e,f) South America (SAm), and (g,h) Middle East (ME) during daytime (left column) and nighttime (right column).  $\Delta W_{ca}$  and  $\Delta W_2$  are represented by yellow and brown bars over daytime and by blue and dark blue bars over nighttime. GFDL represents the simulated  $\Delta W_{ca}$  and  $\Delta W_2$  by the numerical model. TRM represents the sum of the four contributions calculated from the TRM method.  $\alpha$ ,  $r_a$ ,  $r_s$ , G, and  $r'_a$  represent the contributions from albedo, aerodynamic resistance between the surface and the atmosphere, surface resistance, heat storage, and aerodynamic resistance between the 2-m level and the atmosphere, respectively. The error bars are the standard error and indicate the spatial variability.

regional averages of  $\Delta T_2$  and  $\Delta W_2$  mostly vanish during the day except for Central America and West Africa while exhibiting weakly positive signals at night. Note that the error bars are very large especially for regions with negative  $\Delta T_2$  and  $\Delta W_2$ , indicating significant spatial variability within each region. After case-by-case investigations of all 11 regions, we select North America, Central America, South America, and the Middle East to highlight four distinctive regional patterns of the urban-rural differences in heat stress and their attributions (Fig. 10). The results for the urban-rural differences in temperature are presented in Fig. S9 in the Supplementary Materials.

Starting off from the canopy air level, in North America, surface resistance  $(r_s)$  is the leading cause 509 of the positive  $\Delta T_{ca}$  during the daytime (Fig. S9a), indicating the dominant role of evapotranspiration in controlling the urban-rural differences in canopy air temperature in this region. Such results 511 are consistent with the finding of previous studies that the relationship between surface UHI and 512 background climate is largely explained by evapotranspiration (Li et al. 2019; Manoli et al. 2019). For daytime W<sub>ca</sub> (Fig. 10a), the contribution of surface resistance remains strong but aerodynamic 514 resistance plays an equally important role. Heat storage (G) has a strong negative effect (Fig. S9a 515 and Fig. 10a). When the negative contribution of heat storage exceeds the positive contribution of surface resistance, daytime urban-rural contrasts of  $T_{ca}$  and  $W_{ca}$  become negative, as in the case 517 of Central America (Fig. S9c and Fig. 10c) and other regions with negative temperature/SWBGT 518 differences (not shown). Close inspection reveals that the numerical model prescribes very large 519 thermal admittance for urban roofs in these regions (Jackson et al. 2010; Oleson et al. 2011; Oleson and Feddema 2020; Wang et al. 2020a). Since the capability of a surface in storing heat is 521 largely governed by thermal admittance, this explains why these regions have very strong negative 522 contributions from heat storage during the daytime.

In South America (Fig. S9e and Fig. 10e), the positive effect from aerodynamic resistance  $(r_a)$  to 524  $\Delta T_{ca}$  and  $\Delta W_{ca}$  becomes very large and even exceeds that from surface resistance in terms of  $\Delta W_{ca}$ 525 during the daytime, which leads to positive  $\Delta T_{ca}$  and  $\Delta W_{ca}$ . In contrast, aerodynamic resistance  $(r_a)$  makes a large negative contribution in the Middle East (Fig. S9g and Fig. 10g), causing  $\Delta T_{ca}$ 527 and  $\Delta W_{ca}$  to be negative. These results are broadly consistent with recent work on the spatial 528 variability of daytime surface UHI (Zhao et al. 2014; Li et al. 2019; Manoli et al. 2019). Cities in 529 humid climates (South America) are often surrounded by forests, which might convect heat more efficiently than buildings. Hence aerodynamic resistance makes a positive contribution to daytime 531  $\Delta T_{ca}$  and  $\Delta W_{ca}$ . On the other hand, in dry regions (Middle East) rural areas are characterized 532 by short vegetation and deserts and cities can have a higher convection efficiency, as discussed in Section 3.b. As a result, the contribution from aerodynamic resistance becomes strongly negative 534 and the positive contribution from surface resistance is weak in these dry regions, which therefore 535 causes negative daytime  $\Delta T_{ca}$  and  $\Delta W_{ca}$ .

During the night, the attribution results are more consistent across different regions (e.g., North America, Central America, and South America), characterized by a dominant positive contribution from the ground heat storage and thus positive  $\Delta T_{ca}$  and  $\Delta W_{ca}$  (see Fig. S9b,d,f and Fig. 10b,d,f). However, in the Middle East, the negative effect of aerodynamic resistance exceeds the positive effect of heat storage release, resulting in negative  $\Delta T_{ca}$  and  $\Delta W_{ca}$ .

Concerning the 2-m level results, the urban-rural contrast of all variables becomes nearly zero during the day regardless of regions as a result of strong mixing (Fig. S9a, c, e, g and Fig. 10a, c, e, g). Similar to what was found in Venter et al. (2021) and Stewart et al. (2021), the magnitude of the simulated  $\Delta T_{ca}$  (which is closer to the surface UHI in the observations) far exceeds that of  $\Delta T_2$  (which is closer to the near-surface UHI in the observations). At night the primary heat source of the near atmosphere comes from heat storage accumulated in the daytime (Oke et al. 2017; Grimmond and Oke 1999). As a result, these 4 regions have slightly positive  $\Delta T_2$  and  $\Delta W_2$  during the night, with a magnitude much less than their canopy air counterparts.

### 50 4. Conclusions

In this study, we develop a methodology to quantify the physical processes contributing to the 551 urban-rural difference in heat stress based on the Two-Resistance Mechanism (TRM) method. 552 The improved TRM method is applied to diagnosing urban-rural contrast of canopy air temper-553 ature/SWBGT simulated by the GFDL LM4.0 coupled with a UCM. Results indicate that con-554 tributions of the four biophysical factors (albedo, aerodynamic resistance, surface resistance, and ground heat flux or heat storage) to the urban-rural differences in canopy air SWBGT ( $\Delta W_{ca}$ ) vary 556 diurnally and geographically. The urban-rural contrasts of canopy air SWBGT ( $\Delta W_{ca}$ ) and canopy 557 air temperature ( $\Delta T_{ca}$ ) share similarity, but the magnitude of  $\Delta W_{ca}$  is smaller due to moisture deficits in cities. 559

We further apply the attribution framework to study four different regions (North America, Central America, South America, and the Middle East). In North America, surface resistance makes a stronger contribution than ground heat flux during the daytime, while it is the opposite in Central America. Aerodynamic resistance can make positive (e.g., North America and South America), negligible (e.g., Central America), or negative (e.g., Middle East) contributions during the daytime. The nighttime results are more consistent across geographic regions with mostly

positive urban-rural differences in temperatures and heat stresses due to the strongly positive contributions from heat storage. Only in the Middle East does the negative contribution of aerodynamic resistance overweight the positive contribution from ground heat flux at night.

We also extend the method to studying the 2-m air temperature/SWBGT. A new biophysical factor, the 2-m level aerodynamic resistance ( $r'_a$ ), is introduced in the attribution framework. Overall,  $\Delta W_2$  and  $\Delta T_2$  share similar patterns as  $\Delta W_{ca}$  and  $\Delta T_{ca}$ , respectively, but with much smaller magnitude due to turbulent mixing in the surface layer.

### 5. Discussions

582

583

585

586

587

This study has several implications that are important to appreciate. First, the methodology to quantitatively attribute urban-rural differences in heat stress is generic and can be applied to any heat stress index that is a function of temperature and humidity. Therefore, it allows for the intercomparison of different heat stress indices as well as the intercomparison of different numerical models. However, we caution that this method is not applicable to heat indices that are also functions of radiation and wind speed. Further development of attribution methods for more complicated heat stress indices is still needed.

Second, the traditional definition of 2-m air temperature and heat stress does not necessarily facilitate a clean comparison between urban and rural thermal conditions. Since urban areas often have a much larger displacement height, the so-called '2-m' air temperature (and heat stress) correspond to a higher physical height in urban areas than in rural areas. This might partly explain why the model yields negative daytime urban-rural differences in heat stress. Some models try to correct such effects in an ad-hoc way but it remains unclear what constitutes a clean comparison in numerical models that do not resolve the temperature/humidity profiles within the urban canopy.

Third, the attribution method used in this study highlights two well-known causes of the positive urban-rural differences in temperatures and heat stresses: the lack of evapotranspiration (a daytime effect) and the stronger release of heat storage (a nighttime effect). However, the daytime urban-rural contrasts of canopy air temperature and heat stress are found to be negative in places where urban areas are surrounded by short vegetation (e.g., arid regions) so that urban areas have lower aerodynamic resistances and in places where urban materials have very large thermal admittance.

These factors have been less studied but are physically possible. They highlight that it is critical

for numerical models to prescribe the correct roughness lengths and thermal properties to capture
the urban-rural contrasts of temperature and heat stress.

Fourth, while the attribution method can shed many insights, applying it to diagnosing numerical 597 model outputs should proceed with caution. The attribution method is developed for a bulk surface. However, numerical models often treat urban (and rural) areas as having multiple heat sources and 599 sinks. As a result, it is not straightforward to construct a bulk surface temperature using numerical 600 model outputs. Extending the TRM attribution method to the 2-m level is more challenging. As the magnitude of simulated urban-rural differences in temperature and heat stress at the 2-m 602 level is smaller, the TRM modeled urban-rural differences in temperature and heat stress at the 603 2-m level are more scattered. Moreover, some parameters needed by the attribution method and inferred from numerical model outputs (e.g., aerodynamic resistance) might become physically 605 meaningless (e.g., aerodynamic resistance is negative). The current practice is to simply discard 606 such data. Further developments of attribution methods are needed to verify the consequence of 607 the such practice.

Last but not least, it's worth noting that the attribution method, as a diagnostic method, does not provide any information regarding the validity of the numerical model results against real-world observations. Validation against observations is outside the scope of this study but is critical for establishing confidence in the numerical model results.

- 613 Acknowledgments. The authors are grateful to Dr. Keith Oleson at NCAR for insightful dis-
- cussions. YQ and DL acknowledge support from the U.S. National Science Foundation (Grant
- ICER-1854706). WL acknowledges support from the National Natural Science Foundation of
- china (Grants 42271419, 41901327, and 42075070).
- Data availability statement. All data used in this analysis are publicly available at https:
- //doi.org/10.5281/zenodo.6629390, or by request to the corresponding author.

#### 619 References

- Anderson, G. B., M. L. Bell, and R. D. Peng, 2013: Methods to calculate the heat index as an
- exposure metric in environmental health research. Environmental Health Perspectives, 121 (10),
- 622 1111–1119, https://doi.org/10.1289/ehp.1206273.
- Barriopedro, D., E. M. Fischer, J. Luterbacher, R. M. Trigo, and R. García-Herrera, 2011: The
- hot summer of 2010: Redrawing the temperature record map of Europe. Science, 332 (6026),
- 625 220–224, https://doi.org/10.1126/science.1201224.
- Best, M., and C. Grimmond, 2015: Key conclusions of the first international urban land surface
- model comparison project. Bull. Amer. Meteor. Soc., 96 (5), 805–819, https://doi.org/10.1175/
- BAMS-D-14-00122.1.
- Bonan, G., 2019: Climate Change and Terrestrial Ecosystem Modeling. Cambridge University
- eso Press, 437 pp.
- Buzan, J. R., K. Oleson, and M. Huber, 2015: Implementation and comparison of a suite of heat
- stress metrics within the Community Land Model version 4.5. *Geoscientific Model Development*,
- 8 (2), 151–170, https://doi.org/10.5194/gmd-8-151-2015.
- 684 Carnahan, W. H., and R. C. Larson, 1990: An analysis of an urban heat sink. Remote sensing of
- Environment, **33** (1), 65–71, https://doi.org/10.1016/0034-4257(90)90056-R.
- <sup>656</sup> Chakraborty, T., Z. S. Venter, Y. Qian, and X. Lee, 2022: Lower urban humidity moderates
- outdoor heat stress. AGU Advances, 3 (5), e2022AV000729, https://doi.org/https://doi.org/10.
- 638 1029/2022AV000729.

- Chen, C., L. Wang, R. B. Myneni, and D. Li, 2020: Attribution of land-use/land-cover change induced surface temperature anomaly: How accurate is the first-order Taylor series expansion?
   Journal of Geophysical Research: Biogeosciences, 125 (9), e2020JG005 787, https://doi.org/https://doi.org/10.1029/2020JG005787.
- Chen, L., and P. A. Dirmeyer, 2016: Adapting observationally based metrics of biogeophysical
   feedbacks from land cover/land use change to climate modeling. *Environmental Research Letters*,
   11 (3), 34 002—-34 015, https://doi.org/10.1088/1748-9326/11/3/034002.
- Dunne, J. P., R. J. Stouffer, and J. G. John, 2013: Reductions in labour capacity from heat stress under climate warming. *Nature climate change*, **3** (**6**), 563–566, https://doi.org/10.1038/nclimate1827.
- Dupont, E., L. Menut, B. Carissimo, J. Pelon, and P. Flamant, 1999: Comparison between the atmospheric boundary layer in Paris and its rural suburbs during the ECLAP experiment.

  Atmospheric Environment, 33 (6), 979–994, https://doi.org/10.1016/S1352-2310(98)00216-7.
- Fanger, P. O., 1972: *Thermal comfort: Analysis and applications in environmental engineering.*McGraw-Hill, 244 pp.
- Fischer, E. M., K. W. Oleson, and D. M. Lawrence, 2012: Contrasting urban and rural heat stress responses to climate change. *Geophys. Res. Lett.*, **39** (3), https://doi.org/10.1029/2011GL050576.
- Garratt, J., 1994: *The Atmospheric Boundary Layer*. Cambridge Atmospheric and Space Science Series, Cambridge University Press, 316 pp.
- Grimmond, C. S. B., and T. R. Oke, 1999: Heat storage in urban areas: Local-scale observations and evaluation of a simple model. *J. Appl. Meteor. Climatol.*, **38** (7), 922, https://doi.org/
- Grimmond, C. S. B., and Coauthors, 2010: The international urban energy balance models
   comparison project: First results from Phase 1. *J. Appl. Meteor. Climatol.*, 49 (6), 1268–1292,
   https://doi.org/10.1175/2010JAMC2354.1.
- Grimmond, C. S. B., and Coauthors, 2011: Initial results from Phase 2 of the international urban energy balance model comparison. *Int. J. Climatol.*, **31** (2), 244–272, https://doi.org/

- <sup>667</sup> Grimmond, S., 2007: Urbanization and global environmental change: Local effects of urban
- warming. *The Geographical Journal*, **173** (1), 83–88, https://doi.org/10.1111/j.1475-4959.2007.
- 669 232\_3.x.
- <sup>670</sup> Grundstein, A., and E. Cooper, 2018: Assessment of the Australian Bureau of Meteorology wet bulb
- globe temperature model using weather station data. *International journal of biometeorology*,
- 62 (12), 2205–2213, https://doi.org/https://doi.org/10.1007/s00484-018-1624-1.
- Howard, L., 1833: The Climate of London: Deduced from Meteorological Observations Made in
- the Metropolis and at Various Places Around it, Vol. 3. Harvey and Darton, J. and A. Arch,
- Longman, Hatchard, S. Highley [and] R. Hunter, 383 pp.
- Jackson, P. S., 1981: On the displacement height in the logarithmic velocity profile. *Journal of Fluid Mechanics*, **111**, 15–25, https://doi.org/10.1017/S0022112081002279.
- Jackson, T. L., J. J. Feddema, K. W. Oleson, G. B. Bonan, and J. T. Bauer, 2010: Parameterization
- of urban characteristics for global climate modeling. Annals of the Association of American
- Geographers, **100** (**4**), 848–865, https://doi.org/10.1080/00045608.2010.497328.
- Katul, G. G., A. G. Konings, and A. Porporato, 2011: Mean velocity profile in a sheared and
- thermally stratified atmospheric boundary layer. *Physical review letters*, **107** (**26**), 268 502,
- https://doi.org/10.1103/PhysRevLett.107.268502.
- Kong, Q., and M. Huber, 2022: Explicit calculations of wet-bulb globe temperature com-
- pared with approximations and why it matters for labor productivity. Earth's Future, 10 (3),
- e2021EF002 334, https://doi.org/https://doi.org/10.1029/2021EF002334.
- Kusaka, H., H. Kondo, Y. Kikegawa, and F. Kimura, 2001: A simple single-layer urban canopy
- model for atmospheric models: Comparison with multi-layer and slab models. Boundary-layer
- meteorology, **101** (3), 329–358, https://doi.org/10.1023/A:1019207923078.
- Landsberg, H. E., 1981: *The urban climate*, International geophysics series, Vol. 28. Academic
- <sup>691</sup> Press, 275 pp.
- Li, D., 2021: The O'KEYPS equation and 60 years beyond. Boundary-Layer Meteorology, 179 (1),
- 693 19–42, https://doi.org/10.1007/s10546-020-00585-y.

- Li, D., and E. Bou-Zeid, 2014: Quality and sensitivity of high-resolution numerical simulation of urban heat islands. *Environmental Research Letters*, **9** (**5**), 055 001, https://doi.org/10.1088/
- Li, D., W. Liao, A. J. Rigden, X. Liu, D. Wang, S. Malyshev, and E. Shevliakova, 2019: Urban heat island: Aerodynamics or imperviousness? *Science Advances*, **5** (**4**), eaau4299, https://doi.org/
- Li, D., S. Malyshev, and E. Shevliakova, 2016a: Exploring historical and future urban climate in the earth system modeling framework: 1. model development and evaluation. *J. Adv. Model. Earth Syst.*, **8 (2)**, 917–935, https://doi.org/10.1002/2015MS000578.
- Li, D., S. Malyshev, and E. Shevliakova, 2016b: Exploring historical and future urban climate in the earth system modeling framework: 2. impact of urban land use over the continental united states. *J. Adv. Model. Earth Syst.*, **8 (2)**, 936–953, https://doi.org/10.1002/2015MS000579.
- Liao, W., D. Li, S. Malyshev, E. Shevliakova, H. Zhang, and X. Liu, 2021: Amplified increases of compound hot extremes over urban land in China. *Geophys. Res. Lett.*, **48** (**6**), e2020GL091 252, https://doi.org/10.1029/2020GL091252.
- Liao, W., X. Liu, E. Burakowski, D. Wang, L. Wang, and D. Li, 2020: Sensitivities and responses of land surface temperature to deforestation-induced biophysical changes in two global earth system models. *J. Climate*, **33** (**19**), 8381–8399, https://doi.org/10.1175/JCLI-D-19-0725.1.
- Liao, W., A. J. Rigden, and D. Li, 2018: Attribution of local temperature response to deforestation.
   Journal of Geophysical Research: Biogeosciences, 123 (5), 1572–1587, https://doi.org/10.1029/
   2018JG004401.
- Manoli, G., and Coauthors, 2019: Magnitude of urban heat islands largely explained by climate and population. *Nature*, **573** (**7772**), 55–60, https://doi.org/10.1038/s41586-019-1512-9.
- Masson, V., 2000: A physically-based scheme for the urban energy budget in atmospheric models. *Boundary-layer meteorology*, **94** (**3**), 357–397, https://doi.org/10.1023/A:1002463829265.
- Matthies, F., G. Bickler, S. Hales, and N. C. Marín, 2008: *Heat-Health Action Plans Guidance*.

  World Health Organization, Europe, 45 pp.

- McCarthy, M. P., M. J. Best, and R. A. Betts, 2010: Climate change in cities due to global warming and urban effects. *Geophys. Res. Lett.*, **37** (9), https://doi.org/10.1029/2010GL042845.
- Meili, N., and Coauthors, 2020: An urban ecohydrological model to quantify the effect of vegetation on urban climate and hydrology (ut&c v1. 0). *Geoscientific Model Development*, **13** (1), 335–362, https://doi.org/10.5194/gmd-13-335-2020.
- Middel, A., S. AlKhaled, F. A. Schneider, B. Hagen, and P. Coseo, 2021: 50 grades of shade.
- Bulletin of the American Meteorological Society, **102** (9), E1805 E1820, https://doi.org/
- Monteith, J. L., and M. H. Unsworth, 2008: *Principles of environmental physics*. 3rd ed., Elsevier, 418 pp.
- Moon, M., D. Li, W. Liao, A. J. Rigden, and M. A. Friedl, 2020: Modification of surface energy balance during springtime: The relative importance of biophysical and meteorological changes.

  Agric. For. Meteor., **284**, 107 905, https://doi.org/10.1016/j.agrformet.2020.107905.
- National Weather Service, 2021: Summary of natural hazard statistics for 2020 in the United States. Accessed 7 Jun 2022, https://www.weather.gov/media/hazstat/sum20.pdf.
- Oke, T. R., 1978: Boundary layer climates. Methuen; Wiley, 372 pp.
- Oke, T. R., 1981: Canyon geometry and the nocturnal urban heat island: Comparison of scale model and field observations. *Journal of Climatology*, **1** (**3**), 237–254, https://doi.org/10.1002/joc.3370010304.
- Oke, T. R., 1982: The energetic basis of the urban heat island. *Quart. J. Roy. Meteor. Soc.*, **108 (455)**, 1–24, https://doi.org/10.1002/qj.49710845502.
- Oke, T. R., G. Mills, A. Christen, and J. A. Voogt, 2017: *Urban Climates*. Cambridge University Press, 548 pp.
- Oleson, K., 2012: Contrasts between urban and rural climate in CCSM4 CMIP5 climate change scenarios. *J. Climate*, **25** (**5**), 1390–1412, https://doi.org/10.1175/JCLI-D-11-00098.1.

- Oleson, K., and Coauthors, 2013: Technical description of version 4.5 of the Community Land Model (CLM). NCAR Tech. Note NCAR/TN-503+STR, 434 pp. https://doi.org/
- Oleson, K. W., G. B. Bonan, J. Feddema, and T. Jackson, 2011: An examination of urban heat island characteristics in a global climate model. *Int. J. Climatol.*, **31** (**12**), 1848–1865, https://doi.org/10.1002/joc.2201.
- Oleson, K. W., G. B. Bonan, J. Feddema, and M. Vertenstein, 2008a: An urban parameterization for a global climate model. Part II: Sensitivity to input parameters and the simulated urban heat island in offline simulations. *J. Appl. Meteor. Climatol.*, **47** (**4**), 1061 1076, https://doi.org/
- Oleson, K. W., G. B. Bonan, J. Feddema, M. Vertenstein, and C. S. B. Grimmond, 2008b: An urban parameterization for a global climate model. Part I: Formulation and evaluation for two cities. *J. Appl. Meteor. Climatol.*, **47** (**4**), 1038 1060, https://doi.org/10.1175/2007JAMC1597.1.
- Oleson, K. W., and J. Feddema, 2020: Parameterization and surface data improvements and new capabilities for the Community Land Model Urban (CLMU). *J. Adv. Model. Earth Syst.*, **12 (2)**, e2018MS001 586, https://doi.org/10.1029/2018MS001586.
- Oleson, K. W., A. Monaghan, O. Wilhelmi, M. Barlage, N. Brunsell, J. Feddema, L. Hu, and D. F. Steinhoff, 2015: Interactions between urbanization, heat stress, and climate change. *Climatic Change*, **129** (**3-4**), 525–541, https://doi.org/10.1007/s10584-013-0936-8.
- Rigden, A. J., and D. Li, 2017: Attribution of surface temperature anomalies induced by land use and land cover changes. *Geophys. Res. Lett.*, **44** (**13**), 6814–6822, https://doi.org/10.1002/2017GL073811.
- Robine, J.-M., S. L. K. Cheung, S. Le Roy, H. Van Oyen, C. Griffiths, J.-P. Michel, and F. R. Herrmann, 2008: Death toll exceeded 70,000 in Europe during the summer of 2003. *Comptes Rendus Biologies*, **331** (2), 171–178, https://doi.org/10.1016/j.crvi.2007.12.001.
- Seto, K. C., and J. M. Shepherd, 2009: Global urban land-use trends and climate impacts. *Current opinion in environmental sustainability*, **1** (1), 89–95, https://doi.org/10.1016/j.cosust.2009.07.

- Sheffield, J., G. Goteti, and E. F. Wood, 2006: Development of a 50-year high-resolution global dataset of meteorological forcings for land surface Modeling. *J. Climate*, **19** (**13**), 3088–3111, https://doi.org/10.1175/JCLI3790.1.
- Sherwood, S. C., and M. Huber, 2010: An adaptability limit to climate change due to heat stress. *Proceedings of the National Academy of Sciences*, **107** (**21**), 9552–9555, https://doi.org/
- Stewart, I., E. Krayenhoff, J. Voogt, J. Lachapelle, M. Allen, and A. Broadbent, 2021: Time evolution of the surface urban heat island. *Earth's Future*, 9 (10), e2021EF002178, https://doi.org/10.1029/2021EF002178.
- Stull, R. B., 1988: *An Introduction to Boundary Layer Meteorology*, Vol. 13. Springer Science & Business Media, 670 pp.
- Uno, I., S. Wakamatsu, H. Ueda, and A. Nakamura, 1992: Observed structure of the nocturnal urban boundary layer and its evolution into a convective mixed layer. *Atmospheric Environment*.

  Part B. Urban Atmosphere, **26** (**1**), 45–57, https://doi.org/10.1016/0957-1272(92)90036-R.
- Venter, Z. S., T. Chakraborty, and X. Lee, 2021: Crowdsourced air temperatures contrast satellite measures of the urban heat island and its mechanisms. *Science Advances*, **7** (22), eabb9569, https://doi.org/10.1126/sciadv.abb9569.
- Wang, L., M. Huang, and D. Li, 2020a: Where are white roofs more effective in cooling the surface? *Geophys. Res. Lett.*, **47** (**15**), e2020GL087 853, https://doi.org/10.1029/2020GL087853.
- Wang, L., and D. Li, 2021: Urban heat islands during heat waves: A comparative study between
  Boston and Phoenix. *J. Appl. Meteor. Climatol.*, https://doi.org/10.1175/JAMC-D-20-0132.1.
- Wang, L., D. Li, N. Zhang, J. Sun, and W. Guo, 2020b: Surface urban heat and cool islands and their drivers: An observational study in Nanjing, China. *J. Appl. Meteor. Climatol.*, **59** (**12**), 1987–2000, https://doi.org/10.1175/JAMC-D-20-0089.1.
- Wang, P., D. Li, W. Liao, A. Rigden, and W. Wang, 2019: Contrasting evaporative responses of ecosystems to heatwaves traced to the opposing roles of vapor pressure deficit and surface resistance. *Water Resources Research*, **55** (6), 4550–4563, https://doi.org/10.1029/2019WR024771.

- Willett, K. M., and S. Sherwood, 2012: Exceedance of heat index thresholds for 15 regions under a warming climate using the wet-bulb globe temperature. *Int. J. Climatol.*, **32** (2), 161–177, https://doi.org/10.1002/joc.2257.
- World Meterological Organization, 2021: June ends with exceptional heat. Accessed 8 October 2021, https://public.wmo.int/en/media/news/june-ends-exceptional-heat.
- Yow, D. M., 2007: Urban heat islands: Observations, impacts, and adaptation. *Geography compass*,
   1 (6), 1227–1251, https://doi.org/10.1111/j.1749-8198.2007.00063.x.
- Zhang, Y., I. Held, and S. Fueglistaler, 2021: Projections of tropical heat stress constrained by atmospheric dynamics. *Nature geoscience*, **14** (**3**), 133–137, https://doi.org/10.1038/s41561-021-00695-3.
- Zhao, L., X. Lee, R. B. Smith, and K. Oleson, 2014: Strong contributions of local background climate to urban heat islands. *Nature*, **511** (**7508**), 216–219, https://doi.org/10.1038/nature13462.